# Finite Kinematics in Radiative Energy Loss

A. G. Renecle, W. A. Horowitz, M. Lushozi

*Department of Physics, University of Cape Town, Rondebosch 7701, South Africa*



**Abstract**

We investigate the behaviour of particle emission spectra in the large-$x$ region derived from a rigorous implementation of the exact kinematic constraints in the framework of a scalar model of radiative emissions. We find that the small-$x$ kinematic constraints in the simpler theory are identical to those implemented in sophisticated QCD-based energy loss models, but that the exact large-$x$ kinematics in the toy theory are more complicated than those implemented in those same QCD-based energy loss models. We compute the differential cross-section for various values of the parent parton energy and see that our spectra respect energy conservation by smoothly vanishing outside the classically allowed $0 < x < 1$ region.

*Keywords:* Bremsstrahlung, Kinematics, Large-$x$, Radiative Energy Loss

## 1. Introduction

The goal of jet tomography in high-energy nuclear physics is the quantitative measurement of the non-trivial, emergent, many-body dynamics of QCD using hard probes of high-energy collision experiments [1]. Experiments from $\sqrt{s} \sim 0.2 - 5.5$ ATeV have definitively demonstrated a significant modification of the hard spectrum of particles in nucleus-nucleus collisions compared to proton-proton collisions, and numerous works have shown a qualitative description of this wealth of data [2–9].

In order to perform quantitative jet tomography, one requires a well-controlled theoretical understanding of the energy loss processes associated with the hard probe of a heavy ion collision. Since hard processes involve a hard scale, often the energy of a very high-momentum $\sim 100$ GeV, it's

*Email address:* rncant003@myuct.ac.za (A. G. Renecle)

not unreasonable to think that perturbative methods can be applied to the problem. Under the assumption of perturbative QCD (pQCD) applied to energy loss processes, there are two energy loss channels: elastic (or collisional) and inelastic (or radiative). In heavy ion collisions, both radiative and collisional energy losses scale with the log of the momentum of the parton—the typical linear scaling of radiative energy loss is softened to logarithmic from the LPM effect [10–12]—but the radiative losses are about 3 times larger than the collisional [13].

Often, the key quantity used in the determination of pQCD radiative energy loss is the single inclusive radiated gluon distribution $dN_g/dxdk_T^2$, where $x$ is the energy fraction taken from the emitting hard parton by the emitted gluon and $k_T$ is the perpendicular momentum of the emitted gluon. Superficially, this radiation kernel sets the mean energy lost by a high momentum particle, $\langle \Delta E \rangle = \int dxdk_T^2\, xE\, dN_g/dxdk_T^2$. More sophisticated energy loss models treat the radiative energy loss more carefully, but, ultimately, the calculations rely on the radiative kernel $dN_g/dxdk_T^2$.

When computing $dN_g/dxdk_T^2$ one evaluates diagrams with a single emitted gluon. However, the calculation is inclusive: the final state of the process—other than the emitted gluon—is integrated over. There are two important consequences of deriving an inclusive expression. First, the derivation doesn't naturally enforce exact kinematics. Second, the number of emitted gluons isn't actually fixed; $\int dxdk_T^2 dN_g/dxdk_T^2 \neq 1$.

Practically, energy loss modellers impose finite kinematics on the energy loss formulae *a posteriori*, generally of the form of a $q_T^{\max} \sim \sqrt{6ET}$ associated with the largest $2 \to 2$ $t$-channel exchange process between a parton of energy and momentum $\sim E$ and a medium particle of energy and momentum $\sim 3\mu_D$, where $\mu_D \sim gT$ is the Debye screening mass of the plasma, and of $k_T^{\max} \sim xE$ or $\sim x(1-x)E$ [14]. $k_T^{\max} \sim xE$ forces the gluon to be emitted in the forward direction and $k_T^{\max} \sim (1-x)E$ forces the emitting hard parton to continue propagating in the forward direction. Often the energy loss derivation assumes that the radiated gluon is both soft ($x \ll 1$) and collinear ($k_T \ll xE$); a choice of $k_T^{\max} \sim xE$ for small $x$ has the added benefit of enforcing a limit on the acollinearity of the emitted gluon.

Many works [15–17] have repeatedly demonstrated that a loose treatment of kinematics (e.g. by treating the kinematics as infinite or through not carefully treating the finite kinematics) can make an enormous difference in predictions for phenomenologically relevant observables. It's therefore worth considering the effects of exact finite kinematics in an exactly solvable, to

leading order, model of radiative emissions, which is the main purpose of this work.

Since the number of emitted gluons isn't fixed for the single inclusive gluon spectrum $dN_g/dxdk_T^2$, one is able to determine the average number of emitted gluons, $\langle N_g \rangle = \int dxdk_T^2 dN_g/dxdk_T^2$. The average number of bremsstrahlung gluons emitted by a high momentum parton in a central heavy ion collision is $\sim 3$ [18]. It's therefore important to include the effect of emitting several gluons. However, emitting several gluons compounds the difficulties associated with finite kinematics since the usual treatments involving multiple gluon emissions further neglect to enforce total energy and momentum conservation. For a wide range of parton paths, the probability of losing a fraction of energy greater than 1 has significant support. Several methods have been proposed for dealing with this violation of energy conservation [14, 16, 19]; the work done here provides some insight on a careful treatment of this energy conservation violating probability.

A few questions naturally arise related to the exact kinematics. When $dN_g/dxdk_T$ is computed in the usual way, assuming an inclusive process and that the emitted gluon is soft and collinear, the amplitude has non-zero support in regions that are kinematically forbidden. In an exact calculation, does the amplitude know about the kinematics and have support only in the kinematically allowed region? We will show that an exactly computed amplitude is ignorant of the kinematics; i.e. even an exactly computed amplitude has support in kinematically forbidden regions. Second, how do the usual *a posteriori* kinematic constraints used in energy loss phenomenology compare to the kinematic constraints in an exact calculation? Ideally, one would hope that the kinematic constraints imposed *a posteriori* emerge naturally from a full kinematic treatment. We will see that for our simple model, the small-$x$ kinematic constraints are identical with the *a posteriori* constraints, but that the exact kinematics are more complicated at large-$x$ than the usual constraints imposed in energy loss models.

In order to investigate the effect of exactly treating the finite kinematics associated with radiative emissions, we focus, for simplicity, on the vacuum radiation associated with hard scattering. In order to further simplify our model, we consider only scalar particles. In the last simplification, we allow the radiated particle to only couple to one of the outgoing legs, so that only a single amplitude need be considered.

The thesis is organized as follows. In Sec. 2 we review the usual soft and collinear treatment of vacuum radiation associated with a hard scattering

event in QCD. In Sec. 3 we introduce our scalar particle model for computing vacuum radiation exactly after a hard $2 \to 2$ collision, and in Sec. 4 we perform the computation of the total cross-section for a hard $2 \to 2$ collision in our model. In Sec. 5, we compute the differential cross-section for the emission of a scalar particle after a hard $2 \to 2$ collision in our scalar model of radiative emissions, and discuss our findings in more detail in Sec. 6. Finally, we sum up the work performed here in Sec. 7.

## 2. Review of Single Inclusive Soft and Collinear Vacuum Radiation in QCD

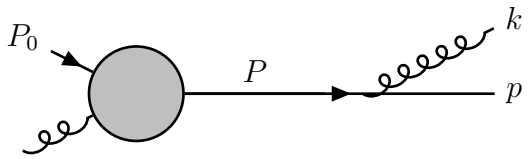


Figure 1: The one diagram to evaluate in computing the single inclusive radiated gluon distribution $dN_g/dxdk_T^2$ associated with a hard $2 \to 3$ scattering event in pQCD. The diagram provides a simplified scheme for calculating the single inclusive radiated gluon distribution $dN_g/dxdk_T^2$ associated with a hard $2 \to 3$ scattering event in pQCD; while the diagram may initially appear to depict a $2 \to 2$ process, the blob encapsulates all elements beyond the outgoing leg and its collinear radiated gluon. This simplification is valid because the radiated gluon is assumed to be collinear to the outgoing leg. These configurations are particularly significant due to the enhancement by a nearly on-shell internal propagator, further elaborated in the main text.

In a typical $2 \to 3$ process in pQCD, at leading order the emitted gluon can attach to any one of the four external legs or the internal propagator. If we assume that the radiated gluon is collinear to one of the external legs, say leg 1, then we may neglect the contribution from the four diagrams in which the gluon is not attached to the outgoing leg 1; the diagram in which the outgoing gluon and leg are collinear is enhanced by a nearly on-shell internal propagator. If we take the process to be inclusive, we may replace everything in the diagram other than the outgoing leg 1 and its radiated gluon with a blob; see Fig. (1).

Firstly, let us define our assumed parameterization of the kinematics for massless QCD. Although the four vectors are in Minkowksi coordinates, $p^\mu \equiv (p^0, p^3, p^1, p^2)^\mu \equiv (p^0, \vec{p})^\mu \equiv (p^0, p^3, \boldsymbol{p})^\mu$, to make easy contact with

[13, 20] the gluon is in lightcone gauge:

$$\begin{aligned} P^\mu &= p^\mu + k^\mu \simeq (E, E, \mathbf{0})^\mu \\ p^\mu &= \left((1-x)E, \sqrt{(1-x)^2E^2 - \boldsymbol{k}^2}, -\boldsymbol{k}\right)^\mu \\ k^\mu &= \left(xE, \sqrt{(xE)^2 - \boldsymbol{k}^2}, \boldsymbol{k}\right)^\mu \\ \epsilon^{*\mu} &\simeq \left(\frac{1}{2}\frac{\boldsymbol{k}\cdot\boldsymbol{\epsilon}}{xE}, -\frac{1}{2}\frac{\boldsymbol{k}\cdot\boldsymbol{\epsilon}}{xE}, \boldsymbol{\epsilon}\right)^\mu. \end{aligned} \tag{1}$$

In the above, we've assumed that the gluon is soft, $x \ll 1$, and collinear, $\boldsymbol{k}^2 \ll (k^z)^2 = (xE)^2 - \boldsymbol{k}^2 \simeq (xE)^2$. We've chosen to use $x$ as the fraction of energy taken by the gluon; in the notation of [16], $x \equiv x_E$.

Our polarization vector in Eq. (1) was derived as follows. We require that $\epsilon^{*\mu}k_\mu = 0$, and that $\epsilon^+ \equiv \epsilon^0 + \epsilon^3 = 0$ since the gluon is assumed to be in lightcone gauge. Supposing that $\epsilon^{*\mu} = (\epsilon^0, \epsilon^3, \boldsymbol{\epsilon})^\mu$, $\epsilon^{*\mu}k_\mu = 0$

$$\begin{aligned} &\Leftrightarrow \epsilon^0(xE) - \epsilon^3\sqrt{(xE)^2 - \boldsymbol{k}^2} - \boldsymbol{k}\cdot\boldsymbol{\epsilon} = 0 \\ &\Leftrightarrow \epsilon^0 - \epsilon^3\sqrt{1 - \frac{\boldsymbol{k}^2}{(xE)^2}} = \frac{\boldsymbol{k}\cdot\boldsymbol{\epsilon}}{xE} \\ &\Leftrightarrow \epsilon^0 - \epsilon^3\left(1 - \frac{\boldsymbol{k}^2}{2(xE)^2} + \cdots\right) = \frac{\boldsymbol{k}\cdot\boldsymbol{\epsilon}}{xE} \\ &\Leftrightarrow \epsilon^0 - \epsilon^3 \simeq \frac{\boldsymbol{k}\cdot\boldsymbol{\epsilon}}{xE}, \end{aligned} \tag{2}$$

where in the final line we use that all but the leading order term in the expansion is of order $\boldsymbol{k}^n/(xE)^n$ for $n$ even, and may therefore be neglected in the colliner limit $\boldsymbol{k}^2 \ll (xE)^2$. Thus, a suitable choice for $\epsilon^0$ and $\epsilon^3$ is

$$\begin{aligned} \epsilon^0 &= \frac{1}{2}\frac{\boldsymbol{k}\cdot\boldsymbol{\epsilon}}{xE}, \text{ and} \\ \epsilon^3 &= -\frac{1}{2}\frac{\boldsymbol{k}\cdot\boldsymbol{\epsilon}}{xE}. \end{aligned} \tag{3}$$

Notice how this choice also satisfies $\epsilon^+ \equiv \epsilon^0 + \epsilon^3 = 0$ as required, so we may take $\epsilon^{*\mu}$ as defined in Eq. (1).

Next, computing the one diagram as given in Fig. (1), one has to leading

order in strong coupling $g$

$$
\begin{aligned}
i\mathcal{M} &= \bar{u}(p)\big(i\,g\,t^a \not{\epsilon}^{a*}(k)\big)\frac{i\not{P}}{P^2}\mathcal{M}_0(P,P_0)u(P_0)\cdots \\
&= \bar{u}(p)\big(i\,g\,t^a \not{\epsilon}^{a*}(k)\big)\frac{i(\not{p}+\not{k})}{P^2}\mathcal{M}_0(P,P_0)u(P_0)\cdots
\end{aligned}
\tag{4}
$$

In the first line we simply wrote down the result of applying the usual Feynman rules to the diagram in Fig. (1), and in the second line we use that $P = p + k$. Note that we sum over the repeated index $a$.

We show in Sec. B that we may neglect contributions to the matrix element from $(1/E)\not{\epsilon}\not{k}$, since every component of the matrix $(1/E)\not{\epsilon}\not{p}$ is much larger than the corresponding component of $(1/E)\not{\epsilon}\not{k}$ in the soft and collinear limits.

Our matrix element in Eq. (4) then becomes

$$
\begin{aligned}
i\mathcal{M} &= \bar{u}(p)\big(i\,g\,t^a \not{\epsilon}^{a*}(k)\big)\frac{i(\not{p}+\not{k})}{P^2}\mathcal{M}_0(P,P_0)u(P_0)\cdots \\
&\simeq \bar{u}(p)\big(i\,g\,t^a \not{\epsilon}^{a*}(k)\big)\frac{i\not{p}}{P^2}\mathcal{M}_0(P,P_0)u(P_0)\cdots,
\end{aligned}
\tag{5}
$$

where in the final line we used that component-wise, $(1/E)\not{\epsilon}\not{k} \ll (1/E)\not{\epsilon}\not{p}$ in our assumptions of softness and collinearity. In order to simplify the final line, note that $\not{\epsilon}^{a*}(k)\not{p} = 2p\cdot\epsilon^{a*} - \not{p}\not{\epsilon}^{a*}$. By the massless Dirac equation, $\bar{u}(p)\not{p} = 0$, and so the term containing the factor $\not{p}\not{\epsilon}^{a*}$ vanishes. We are therefore left with

$$
i\mathcal{M} \simeq -g\frac{2p\cdot\epsilon^{a*}}{P^2}\bar{u}(p)t^a\mathcal{M}_0(P,P_0)u(P_0)\cdots \tag{6}
$$

One can now show that

$$
\left\langle|\mathcal{M}|^2\right\rangle \simeq 4C_R g^2\frac{1}{\boldsymbol{k}^2}\left\langle|\mathcal{M}_0\left(P,P_0\right)|^2\right\rangle, \tag{7}
$$

as shown in Sec. C. Using the usual formula for the differential cross-section in terms of the squared matrix element [21], the probability of the process shown in Fig. (1) is

$$
d\sigma(P_0\to p+k) \simeq d\sigma(P_0\to p)\int\frac{d^3k}{(2\pi)^3 2\omega}4C_R g^2\frac{1}{\boldsymbol{k}^2}, \tag{8}
$$

where $d\sigma(P_0 \to p)$ is the elastic cross-section, and we have inserted an additional phase-space integration for the gluon variable $k$. We take $\omega \equiv xE$.

An approximate equality is used in Eq. (8) instead of an exact equality because of the assumptions of softness and collinearity used thus far. Furthermore, note that the expression in Eq. (8) is inclusive; we have not enforced kinematics in the usual way by including an energy-momentum conserving Dirac delta function. Instead, we treat the kinematics *a posteriori* as described in the paragraph following Eq. (13).

Thus, the differential inclusive number of emitted gluons, conditional on the hard scattering process represented by the blob in the figure and by $\mathcal{M}_0(P, P_0)$, is given by

$$\frac{dN^g}{d^3k} \simeq \frac{1}{(2\pi)^3 2\omega} 4C_R g^2 \frac{1}{\boldsymbol{k}^2}. \tag{9}$$

where we simply use that the differential multiplicity distribution is given by the integrand in Eq. (8), and we once again use an approximate equality because the integrand in Eq. (8) was derived assuming that the emitted gluon is soft and collinear.

Next, we make the change of variables $d^3k \to dxd|\boldsymbol{k}|d\phi \to dxd\boldsymbol{k}^2$ up to some Jacobian factor to be computed in the following. We find that

$$\left| \begin{array}{ccc} \frac{\partial k_1}{\partial x} & \frac{\partial k_1}{\partial |\boldsymbol{k}|} & \frac{\partial k_1}{\partial \phi} \\ \frac{\partial k_2}{\partial x} & \frac{\partial k_2}{\partial |\boldsymbol{k}|} & \frac{\partial k_2}{\partial \phi} \\ \frac{\partial k_3}{\partial x} & \frac{\partial k_3}{\partial |\boldsymbol{k}|} & \frac{\partial k_3}{\partial \phi} \end{array} \right| = \frac{xE^2|\boldsymbol{k}|}{\sqrt{(xE)^2 - \boldsymbol{k}^2}}, \tag{10}$$

where we take $k^1 = |\boldsymbol{k}| \cos\phi$, $k^2 = |\boldsymbol{k}| \sin\phi$ and $k^3 = \sqrt{(xE)^2 - \boldsymbol{k}^2}$. Next,

$$\begin{aligned} \frac{xE^2|\boldsymbol{k}|}{\sqrt{(xE)^2 - \boldsymbol{k}^2}} &= \frac{E|\boldsymbol{k}|}{\sqrt{1 - \frac{\boldsymbol{k}^2}{(xE)^2}}} \\ &= \frac{E|\boldsymbol{k}|}{1 - \frac{\boldsymbol{k}^2}{2(xE)^2} + \cdots} \\ &\simeq E|\boldsymbol{k}|, \end{aligned} \tag{11}$$

where in the final line we use that all but the leading order term in the expansion of the denominator are of order $\boldsymbol{k}^n/(xE)^n$ for $n$ even, and may therefore be neglected in the colliner limit $\boldsymbol{k}^2 \ll (xE)^2$. Thus, we see that

$$\begin{aligned} d^3k &\simeq E|\boldsymbol{k}|dxd|\boldsymbol{k}|d\phi \\ &= 2\pi E|\boldsymbol{k}|dxd|\boldsymbol{k}| \\ &= \pi E dxd\boldsymbol{k}^2, \end{aligned} \tag{12}$$

where in the second line we use that our integrand is $\phi$-independent, and in the final line we use that $d\boldsymbol{k}^2 = 2|\boldsymbol{k}|d|\boldsymbol{k}|$. Eq. (9) therefore becomes

$$\frac{dN^g}{dx d\boldsymbol{k}^2} \simeq \frac{C_R \alpha_s}{\pi^2} \frac{1}{x} \frac{1}{\boldsymbol{k}^2}, \tag{13}$$

where $\alpha_s = g^2/(4\pi)$.

Eq. (13) shows the usual Sudakov double logarithmic growth in $x$ and $\boldsymbol{k}^2$ of the soft and collinear radiation. The explosion of soft and collinear radiation *a posteriori* justifies our assumption of soft and collinear radiation, by which we assumed $x \ll 1$ and $|\boldsymbol{k}| \ll xE$. In order to have a sensible total number of emitted gluons, one must introduce IR and UV cutoffs in $x$ and $|\boldsymbol{k}|$. One introduces $x_{\max} = 1$ is by requiring that overall energy is conserved. In the usual way, one fixes the smallest $x$ by invoking some IR scale $\sim \mu$ and setting $x_{\min} = \mu/E$. Similarly, $|\boldsymbol{k}|_{\min} = \mu$. Finally, one imposes $|\boldsymbol{k}|_{\max}$ by requiring that, at minimum, the gluon should be emitted in the forward direction: $|\boldsymbol{k}| < xE$. This forward emission of the gluon is in some sense a minimal requirement for collinear emission [14, 16]. Many thus set $|\boldsymbol{k}|_{\max} = xE$. Should we further require that the hard parent parton also continue moving in the forward direction, then we require that $|\boldsymbol{k}| < (1-x)E$. Combining $|\boldsymbol{k}| < xE$ and $|\boldsymbol{k}| < (1-x)E$ in a smooth way, many set $|\boldsymbol{k}|_{\max} = x(1-x)E$ [14, 16].

We show in Fig. (2) the result of integrating Eq. (13) over $\boldsymbol{k}$ using the two imposed kinematic limits $|\boldsymbol{k}| < xE$ and $|\boldsymbol{k}| < x(1-x)E$,

$$\frac{dN^g}{dx} = \frac{2C_R \alpha_s}{\pi} \frac{1}{x} \log\left(\frac{|\boldsymbol{k}|_{\max}}{|\boldsymbol{k}|_{\min}}\right). \tag{14}$$

We stop plotting the distribution $dN^g/dx$ once the distribution goes negative. For the limit $|\boldsymbol{k}| < xE$, there is an induced $x_{\min} = |\boldsymbol{k}|_{\min}/E$. For $|\boldsymbol{k}| < x(1-x)E$ there is an induced

$$\begin{aligned} x_{\min} &= \frac{1}{2}\left(1 - \sqrt{1 - \frac{4|\boldsymbol{k}|_{\min}}{E}}\right) \\ x_{\max} &= \frac{1}{2}\left(1 + \sqrt{1 - \frac{4|\boldsymbol{k}|_{\min}}{E}}\right). \end{aligned} \tag{15}$$

One first sees that the $1/x$ divergence is tamed by limiting the $\boldsymbol{k}$ phase space from $|\boldsymbol{k}|_{\max}$. Second, although the derivation assumed that the radiation is

soft and collinear, there's significant support for gluon production for large $x > 0.5$. In fact, one can see that the amplitude yields a probability with support out to $x \to \infty$. It's only when we impose the restriction that the hard emitting parton continue moving forward that the gluon distribution is cut off at a physically reasonable $x_{\max} < 1$.

We will see a similar story play out in the exact treatment of kinematics below: the minimum value of $x$ is fixed by the small $x$ limit of the $|\boldsymbol{k}|_{\max}$ expression, and the maximum value of $x$ is fixed by requiring the continued forward propagation of the emitting parent parton.

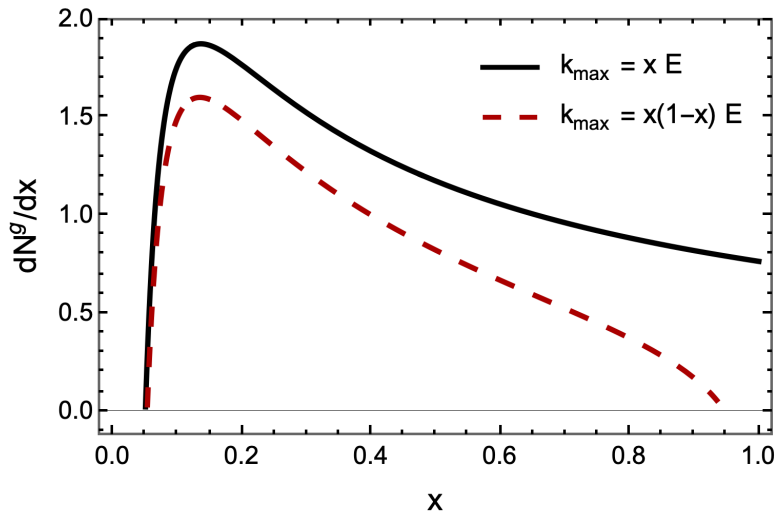


Figure 2: The single inclusive emitted gluon distribution $dN^g/dx$ as a function of $x$ from Eq. (13) for $E = 10$ GeV, $\mu = 0.5$ GeV, $C_R = 4/3$, $\alpha_s = 0.3$ for two different upper bounds $|\boldsymbol{k}|_{\max} = xE$ or $|\boldsymbol{k}|_{\max} = x(1-x)E$. The plots are cut off in $x$ once $dN^g/dx = 0$.

## 3. Model

In order to investigate the effects of finite kinematics in full detail in a fully solved (to leading order) calculation, we introduce a simplified scalar model of gluon bremsstrahlung. Consider a scalar field theory described by the Lagrangian

$$\mathcal{L} \equiv \mathcal{L}_{\text{free}} + \mathcal{L}_{\text{interaction}}, \tag{16}$$

where $\mathcal{L}_{\text{free}} \equiv \mathcal{L}_A + \mathcal{L}_B + \mathcal{L}_C + \mathcal{L}_D$ such that

$$\mathcal{L}_A \equiv \frac{1}{2}\partial_\mu \varphi_A \partial^\mu \varphi_A - \frac{1}{2} m_A^2 \varphi_A^2, \tag{17}$$

and similarly for $A \to B, C, D$. For simplicity, we take $m_A = 0 = m_B$. We take the interaction part of the Lagrangian to be

$$\mathcal{L}_{\text{interaction}} \equiv \frac{1}{6} g_A \varphi_A^3 + g \varphi_A \varphi_B \varphi_C + \frac{1}{2} g_S \varphi_C \varphi_C \varphi_D, \tag{18}$$

where $g, g_A$ and $g_S$ are coupling constants.

## 4. Two-to-Two Scattering

In order to make reasonable contact with the usual single inclusive gluon distribution calculation, we will want to divide out the $2 \to 3$ cross-section that we'll derive in the next section with the $2 \to 2$ cross-section. As a side benefit, exactly computing the $2 \to 2$ cross-section in our model theory serves as a nice warm up to the $2 \to 3$ derivation.

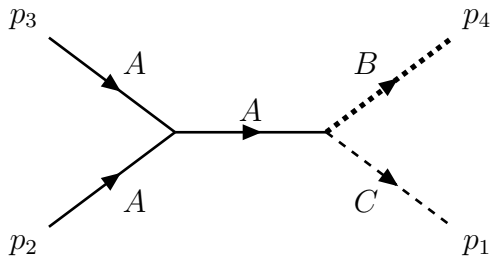


Figure 3: A diagram representing the process of two incoming $A$ particles going to two outgoing particles of type $B$ (dotted line) and $C$ (dashed line).

Consider the matrix element for the two-to-two scattering process $AA \to BC$. This process has a single Feynman diagram; see Fig. (3). The matrix element for this process is

$$\begin{aligned} i\mathcal{M}(AA \to BC) &= (ig_A)(ig)\frac{i}{s} \\ &= -g_A g \frac{i}{s}, \end{aligned} \tag{19}$$

where $s \equiv (p_2 + p_3)^2$ is the usual Mandelstam $s$-variable. We denote the momenta of the two incoming $A$ particles as $p_2^\mu$ and $p_3^\mu$, where, since we assume $m_A = 0$,

$$\begin{aligned} p_2^\mu =& (E, E, \mathbf{0})^\mu, \text{ and} \\ p_3^\mu =& (E, -E, \mathbf{0})^\mu. \end{aligned} \tag{20}$$

We thus have that $s = 2p_2 \cdot p_3 = 4E^2$ in Eq. (19). As for the kinematics of the outgoing particles, we choose that the particles associated with fields $B$ and $C$ have momentum parameterized by

$$\begin{aligned} p_4^\mu =& \left( E_4, \sqrt{E_4^2 - \boldsymbol{p}_4^2}, \boldsymbol{p}_4 \right)^\mu, \text{ and} \\ p_1^\mu =& \left( E_1, \sqrt{E_1^2 - \boldsymbol{p}_1^2 - m_C^2}, \boldsymbol{p}_1 \right)^\mu, \end{aligned} \tag{21}$$

respectively.

The $z$-components of the momenta $p_1, p_2, p_3$ and $p_4$ are fixed by the on-shell condition. We have for the energies of the outgoing particles that

$$\begin{aligned} E_4(\vec{\boldsymbol{p}}_4) &= \sqrt{(p_4^z)^2 + \boldsymbol{p}_4^2}, \text{ and} \\ E_1(\vec{\boldsymbol{p}}_1, m_C) &= \sqrt{(p_1^z)^2 + \boldsymbol{p}_1^2 + m_C^2}. \end{aligned} \tag{22}$$

The differential scattering cross-section [21] for the process $AA \to BC$ is given by

$$\begin{aligned} d\sigma^{2\to 2} = & \frac{(2\pi)^4 \delta^{(4)}(p_2 + p_3 - p_1 - p_4)}{2E_1(\vec{\boldsymbol{p}}_1, m_C) 2E_4(\vec{\boldsymbol{p}}_4) |v_2 - v_3|} \frac{d^3 p_1}{(2\pi)^3 2E_1(\vec{\boldsymbol{p}}_1, m_C)} \frac{d^3 p_4}{(2\pi)^3 2E_4(\vec{\boldsymbol{p}}_4)} \\ & \times |\mathcal{M}(AA \to BC)|^2, \end{aligned} \tag{23}$$

where $v_j$ is the velocity of particle $j$ along the beam. Since the incoming particles are massless, $|v_2 - v_3| = 2$. Thus, the differential cross-section is given by

$$\frac{d\sigma^{2\to 2}}{d^3 p_1 d^3 p_4} = g^2 g_A^2 \frac{1}{2s^3} \frac{1}{2^2 (2\pi)^2} \frac{\delta^{(4)}(p_2 + p_3 - p_1 - p_4)}{E_1(\vec{\boldsymbol{p}}_1, m_C) E_4(\vec{\boldsymbol{p}}_4)}. \tag{24}$$

We can readily perform the integral over $p_4$;

$$\int d^3 p_4 \delta^{(4)}(p_2 + p_3 - p_1 - p_4) = \delta\big(p_2^0 + p_3^0 - p_1^0 - p_4^0\big), \tag{25}$$

where the integral over the spatial Dirac delta function enforces that $\vec{\boldsymbol{p}}_4 = -\vec{\boldsymbol{p}}_1$, such that

$$E_4(\vec{\boldsymbol{p}}_4) = \sqrt{(p_4^z)^2 + \boldsymbol{p}_4^2} = \sqrt{(p_1^z)^2 + \boldsymbol{p}_1^2} = E_4(\vec{\boldsymbol{p}}_1). \tag{26}$$

We now have that

$$\frac{d\sigma^{2\to 2}}{d^3p_1} = g^2 g_A^2 \frac{1}{2s^3} \frac{1}{2^2(2\pi)^2} \frac{1}{E_1(\vec{\boldsymbol{p}}_1, m_C) E_4(\vec{\boldsymbol{p}}_1)} \delta\big(2E - p_1^0 - p_4^0\big). \tag{27}$$

We see that

$$\delta\big(2E - p_1^0 - p_4^0\big) = \delta\left(2E - \sqrt{(p_1^z)^2 + \boldsymbol{p}_1^2 + m_C^2} - \sqrt{(p_1^z)^2 + \boldsymbol{p}_1^2}\right), \tag{28}$$

where we have used that $\vec{\boldsymbol{p}}_4 = -\vec{\boldsymbol{p}}_1$ and that $m_B = 0$. Performing the integral over $p_1^z$, one encounters the expression

$$\begin{aligned}
&\int_{-\infty}^{+\infty} dp_1^z \delta\left(2E - \sqrt{(p_1^z)^2 + \boldsymbol{p}_1^2 + m_C^2} - \sqrt{(p_1^z)^2 + \boldsymbol{p}_1^2}\right) \\
&= \frac{E_1(\vec{\boldsymbol{p}}_1, m_C) E_4(\vec{\boldsymbol{p}}_1)}{2E} \int_{-\infty}^{+\infty} dp_1^z \frac{\delta\left(p_1^z - E\sqrt{\left(1 - \frac{m_C^2}{4E^2}\right)^2 - \frac{\boldsymbol{p}_{1,\perp}^2}{E^2}}\right)}{p_1^z} \\
&= \frac{E_1(\vec{\boldsymbol{p}}_1, m_C) E_4(\vec{\boldsymbol{p}}_1)}{2E^2\sqrt{\left(1 - \frac{m_C^2}{4E^2}\right)^2 - \frac{\boldsymbol{p}_1^2}{E^2}}} \Theta\left(\left(1 - \frac{m_C^2}{4E^2}\right)^2 - \frac{\boldsymbol{p}_1^2}{E^2}\right).
\end{aligned} \tag{29}$$

In the second line, we used that a Dirac delta function composed with a smooth function $g(x)$ with compact support can be rewritten as $\delta(g(x)) = \sum \delta(x - x_i)/|g'(x_i)|$ where $g(x_i) = 0$. We denote the Heaviside theta function by $\Theta$, and choose the positive solution for $p_1^z$. Note the kinematic limit on $|\boldsymbol{p}_1|$ set by our requirement that $p_1^z$ be real:

$$\left(1 - \frac{m_C^2}{4E^2}\right)^2 - \frac{\boldsymbol{p}_1^2}{E^2} > 0, \tag{30}$$

which is to say that

$$|\boldsymbol{p}_1| < E\left(1 - \frac{m_C^2}{4E^2}\right) \tag{31}$$

Note the on-shellness kinematic limit that $m_C < 2E$; we'll assume that $m_C \ll E$. In order to make better contact with the usual QCD calculation, in which one assumes that the gluon radiation is soft and collinear—which is to say that, at minimum, the parent parton continues moving in roughly the same direction after the emission as before—we impose a maximum $|\boldsymbol{p}_1|_{\max} \equiv \xi E$, where $0 < \xi < 1$ is some real number, but is generally speaking $\xi \ll 1$. In general we'll take $m_C \ll 2E$. Hence, with $|\boldsymbol{p}_1|_{\max} \equiv \xi E$, the kinematic limit in Eq. (31) is always satisfied.

The differential cross-section is then

$$\frac{d\sigma^{2\to 2}}{d^2\boldsymbol{p}_1} = \frac{g^2 g_A^2}{2^4(2\pi)^2}\frac{1}{E^2}\frac{1}{s^3}\frac{1}{\sqrt{\left(1-\frac{m_C^2}{4E^2}\right)^2 - \frac{\boldsymbol{p}_1^2}{E^2}}}. \tag{32}$$

The total cross-section is therefore

$$\begin{aligned}\sigma^{2\to 2} &= \int d^2\boldsymbol{p}_1 \frac{d\sigma^{2\to 2}}{d^2\boldsymbol{p}_1} \\ &= \frac{g^2 g_A^2}{2^{13}\pi E^8}\left(4E^2 - m_C^2 - 4E|\boldsymbol{p}_1|_{\max}\sqrt{\frac{(4E^2-m_C^2)^2}{16E^2|\boldsymbol{p}_1|_{\max}^2} - 1}\right),\end{aligned} \tag{33}$$

where we note that since $m_C \ll E$ and $|\boldsymbol{p}_1|_{\max} \ll E$, $(4E^2 - m_C^2)^2 > 16E^2|\boldsymbol{p}_1|_{\max}^2$. Thus, the square root in Eq. (33) is always real.

## 5. Scalar Emission

Consider now the scattering of two particles of species $A$ to three particles of species $B$, $C$, and $D$, where the particle $D$ is emitted off particle $C$. The matrix element for this process again has only a single Feynman diagram, as depicted in Fig. (4).

We choose the kinematics of particles $A$, $B$, and $C$ to be parameterized as in the $2 \to 2$ case. For reference,

$$\begin{aligned} p_2^\mu &= (E, E, \boldsymbol{0})^\mu \\ p_3^\mu &= (E, -E, \boldsymbol{0})^\mu \\ p_4^\mu &= \left(E_4, \sqrt{E_4^2 - \boldsymbol{p}_4^2}, \boldsymbol{p}_4\right)^\mu \\ p_1^\mu &= \left(E_1, \sqrt{E_1^2 - \boldsymbol{p}_1^2 - m_C^2}, \boldsymbol{p}_1\right)^\mu, \end{aligned} \tag{34}$$

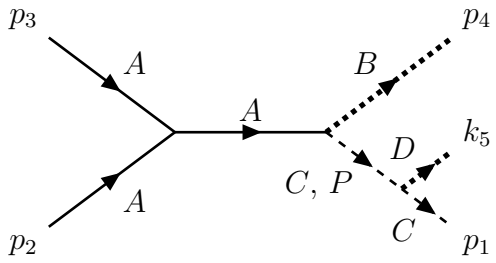


Figure 4: A diagram for the process of two incoming $A$ particles to three particles of type $B$, $C$, and $D$ in our model. The internal $C$ propagator is taken to have momentum $P$.

and we once again have that

$$E_4(\vec{\boldsymbol{p}}_4) = \sqrt{(p_4^z)^2 + \boldsymbol{p}_4^2}, \text{ and}$$
$$E_1(\vec{\boldsymbol{p}}_1, m_C) = \sqrt{(p_1^z)^2 + \boldsymbol{p}_1^2 + m_C^2}. \tag{35}$$

We take the emitted particle $D$ to have momentum

$$k_5^\mu = \left(E_5, \sqrt{E_5^2 - \boldsymbol{k}_5^2 - m_D^2}, \boldsymbol{k}_5\right)^\mu, \quad E_5 \equiv x_5 E. \tag{36}$$

Defined in this way, $x_5$ is the fraction of energy taken away from the emitting particle by the emitted particle. Clearly the $D$ particle is on mass-shell. Requiring $k_5^z$ to be real induces a kinematic constraint,

$$(x_5 E)^2 - \boldsymbol{k}_5^2 - m_D^2 \geq 0. \tag{37}$$

This constraint limits the possible values of $x_5$. Since $|\boldsymbol{k}_5| \geq 0$, we must have

$$x_5 \geq x_{5,\,\text{min}} \equiv \frac{m_D}{E}, \tag{38}$$

Eq. (38) provides a lower bound on the energy of the emitted particle, set by requiring that the emitted particle have at least enough energy to come on mass-shell with rest mass $m_D$.

The matrix element for this process is given by

$$\begin{aligned} i\mathcal{M}(AA \to BCD) &= i\mathcal{M}(AA \to BC)\left(\frac{i}{P^2 - m_C^2}\right)(ig_S) \\ &= igg_A g_S \frac{1}{P^2 - m_C^2}\frac{1}{s}, \end{aligned} \tag{39}$$

where we take $P^\mu \equiv p_1^\mu + k_5^\mu$, such that

$$P^2 = P^2(p_1 \cdot k_5, m_C, m_D) = m_C^2 + m_D^2 + 2p_1 \cdot k_5. \tag{40}$$

The $2 \to 3$ differential cross-section is given by

$$\begin{aligned} d\sigma^{2\to3} = \frac{1}{2s} \frac{d^3p_1}{(2\pi)^3 2E_1(\vec{\boldsymbol{p}}_1, m_C)} \frac{d^3p_4}{(2\pi)^3 2E_4(\vec{\boldsymbol{p}}_4)} \frac{d^3k_5}{(2\pi)^3 2E_5} |\mathcal{M}(AA \to BCD)|^2 \\ \times (2\pi)^4 \delta^{(4)}\left(p_2 + p_3 - p_1 - p_4 - k_5\right). \end{aligned} \tag{41}$$

Hence,

$$\begin{aligned} \frac{d\sigma^{2\to3}}{d^3p_1 d^3k_5} = \frac{\Theta[(k_5^z)^2]}{2s^3} \frac{(gg_S g_A)^2}{(2\pi)^3 2E_1(\vec{\boldsymbol{p}}_1, m_C)} \frac{1}{(2\pi)^3 2} \frac{1}{(2\pi)^3 2E_5} \frac{1}{(P^2 - m_C^2)^2} \\ \times (2\pi)^4 \int d^3p_4 \frac{\delta^{(4)}(p_2 + p_3 - p_1 - p_4 - k_5)}{E_4(\vec{\boldsymbol{p}}_4)}, \end{aligned} \tag{42}$$

where

$$\begin{aligned} \int d^3p_4 \frac{\delta^{(4)}(p_2 + p_3 - p_1 - p_4 - k_5)}{E_4(\vec{\boldsymbol{p}}_4)} \\ = \frac{\delta\big(2E - E_1(\vec{\boldsymbol{p}}_1, m_C) - E_4\big(\vec{\boldsymbol{p}}_1, \vec{\boldsymbol{k}}_5\big) - E_5\big)}{E_4\big(\vec{\boldsymbol{p}}_1, \vec{\boldsymbol{k}}_5\big)}. \end{aligned} \tag{43}$$

The spatial integral over $p_4$ fixes $\vec{\boldsymbol{p}}_4 = -\big(\vec{\boldsymbol{p}}_1 + \vec{\boldsymbol{k}}_5\big)$, and so

$$E_4(\vec{\boldsymbol{p}}_4) = E_4\big(\vec{\boldsymbol{p}}_1, \vec{\boldsymbol{k}}_5\big) = \sqrt{(p_1^z + k_5^z)^2 + \big(\boldsymbol{p}_1 + \boldsymbol{k}_5\big)^2}. \tag{44}$$

Therefore, after performing the spatial integral over $p_4$ and simplifying, the differential cross-section becomes

$$\begin{aligned} \frac{d\sigma^{2\to3}}{d^3p_1 d^3k_5} = \frac{(gg_S g_A)^2}{2^4 s^3 (2\pi)^5} \frac{\Theta[(k_5^z)^2]}{E_1(\vec{\boldsymbol{p}}_1, m_C) E_4\big(\vec{\boldsymbol{p}}_1, \vec{\boldsymbol{k}}_5\big) E_5} \\ \times \frac{\delta\big(2E - E_1(\vec{\boldsymbol{p}}_1, m_C) - E_4\big(\vec{\boldsymbol{p}}_1, \vec{\boldsymbol{k}}_5\big) - E_5\big)}{(P^2 - m_C^2)^2}. \end{aligned} \tag{45}$$

Going forward, we will for the sake of notational simplicity elide the functional dependence of the energies $E_1(\vec{\boldsymbol{p}}_1, m_C) = E_1$ and $E_4(\vec{\boldsymbol{p}}_1, \vec{\boldsymbol{k}}_5) = E_4$.

Next,

$$\frac{d\sigma^{2\to 3}}{d^2\boldsymbol{p}_1 d^3k_5} = \frac{(gg_S g_A)^2}{2^4 s^3 (2\pi)^5}\frac{\Theta[(k_5^z)^2]}{E_5}\int_{-\infty}^{+\infty} dp_1^z \frac{\delta\big(2E - E_1 - E_4 - E_5\big)}{E_1 E_4 (P^2 - m_C^2)^2}, \tag{46}$$

where

$$\delta(2E - E_1 - E_4 - E_5) = \sum_{p_{1,0}^z = p_{1,0\pm}^z} \frac{\delta(p_1^z - p_{1,0}^z)}{J}. \tag{47}$$

We have introduced a Jacobian

$$\begin{aligned} J = J\big(\vec{\boldsymbol{p}}_1, \vec{\boldsymbol{k}}_5, m_C, m_D\big) =& \left|\frac{\partial}{\partial p_1^z}(2E - E_1 - E_4 - E_5)\right| \\ =& \frac{p_1^z}{E_1} + \frac{p_1^z + k_5^z}{E_4}. \end{aligned} \tag{48}$$

We take $p_{1,0\pm}^z$ to be the two solutions of the final line in the equation directly below:

$$\begin{aligned} ((2 - x_5)E)^2 - E_1^2 - E_4^2 &= 2E_1 E_4 \\ \Rightarrow [((2 - x_5)E)^2 - E_1^2 - E_4^2]^2 &= 4E_1^2 E_4^2, \end{aligned} \tag{49}$$

which was obtained by squaring and rearranging the equation for the roots of the argument of the energy-conserving delta function in Eq. (47). Putting this together, the integral over $p_1^z$ in Eq. (46) evaluates to

$$\int_{-\infty}^{+\infty} dp_1^z \frac{\delta\big(2E - E_1 - E_4 - E_5\big)}{E_1 E_4 (P^2 - m_C^2)^2} = \sum_{p_1^z = p_{1,0\pm}^z} \frac{J^{-1}}{E_1 E_4 (P^2 - m_C^2)^2}. \tag{50}$$

One obtains a kinematic constraint from the final line in Eq. (49); we require that $((2 - x_5)E)^2 - E_1^2 - E_4^2 > 0$. Since we take $p_{1,0\pm}^z$ to solve the equation in the final line of Eq. (49), we may in principle obtain solutions in which the quantity in the square brackets is negative. But this is unphysical, so in order to ensure that none of our $p_{1,0\pm}^z$'s solve the equation for these unphysical energies, we must include an overall factor

$$\Theta[((2 - x_5)E)^2 - E_1^2 - E_4^2] \tag{51}$$

in our cross-section. One can show that the argument of the theta function in Eq. (51), to leading order in the energy $E$, evaluates to $2E^2(1 - x_5)$, for

both of the solutions $p_1^z = p_{1,0\pm}^z$. Thus, to leading order, the argument of the theta function in Eq. (51) is strictly negative for $x_5 > 1$. The expression for the next-to-leading (NLO) order term is small compared to the leading order term, but highly complicated. Therefore, we can not analytically rule out small positive contributions to the argument of the theta function in Eq. (51). However, numerically, we do not see any positive support for the argument of the theta function in Eq. (51) for $x_5 > 1$. This, together with our lower bound on $x_5$ derived in Eq. (38), strongly suggests that our cross-section has support strictly in the region $m_D/E < x_5 < 1$.

The differential cross-section now becomes

$$\frac{d\sigma^{2\to 3}}{d^2\boldsymbol{p}_1 d^3k_5} = \frac{(gg_S g_A)^2}{2^4 s^3 (2\pi)^5}\frac{\Theta[(k_5^z)^2]}{E_5}\sum_{p_1^z = p_{1,0\pm}^z}\frac{J^{-1}\Theta[((2-x_5)E)^2 - E_1^2 - E_4^2]}{E_1 E_4 (P^2 - m_C^2)^2}. \quad (52)$$

As with the $2 \to 2$ case, we expect kinematic constraints to arise from the integral over the energy conserving Dirac delta function. We now derive these for the case of $2 \to 3$ scattering by solving for $p_{1,0\pm}^z$. Since all energy factors are squared, Eq. (49) is a quadratic polynomial in $p_1^z$. One may collect powers of $p_1^z$ in order to extract the coefficients $a, b$ and $c$ that solve the quadratic equation

$$p_{1,0\pm}^z = \frac{-b \pm \sqrt{b^2 - 4ac}}{2a}, \quad (53)$$

where $c + bp_{1,0\pm}^z + a(p_{1,0\pm}^z)^2 = 0$, with coefficients $a, b, c$ read off from the expression in Eq. (49) after multiplying out and grouping the terms. Using *Mathematica*, we found that

$$\begin{aligned}
a &= 4(4E^2(1-x_5) + \boldsymbol{k}_5^2 + m_D^2),\\
b &= 4k_5^z(4E^2(1-x_5) + m_C^2 + m_D^2 - 2|\boldsymbol{p}_1||\boldsymbol{k}_5|\cos t),\\
c &= -(16E^4(1-x_5)^2 + (m_C^2 + m_D^2)^2)\\
&\quad + 4E^2(\boldsymbol{p}_1^2(2-x_5)^2 - 2m_D^2(1-x_5) + m_C^2(2 - x_5(2-x_5))\\
&\quad + 4|\boldsymbol{p}_1||\boldsymbol{k}_5|\cos t(4E^2(1-x_5) + m_C^2 + m_D^2 - |\boldsymbol{p}_1||\boldsymbol{k}_5|\cos t), \quad (54)
\end{aligned}$$

where $t \in [0, 2\pi)$ is the angle between $\boldsymbol{p}_1$ and $\boldsymbol{k}_5$. We note that $c$ looks almost like a perfect square, but we have confirmed that our expression for $c$ in Eq. (54) is in fact correct; $c$ is not a perfect square.

One notes that in order to ensure measurable results, we must enforce that the discriminant in Eq. (53) is always positive, such that $p_{1,0\pm}^z \in \mathbb{R}$.

Furthermore, we are free to choose that $p^z_{1,0\pm} > 0$, so we will make this choice. We are thus further constrained by the kinematics to impose conditions on the coefficients to ensure that we always take $p^z_{1,0\pm} > 0$. These kinematic constraints are derived by considering cases as follows.

Suppose that $a, b > 0$. We seek to enforce that $p^z_{1,0\pm} > 0$. Since $a > 0$, we need only enforce that $-b \pm \sqrt{b^2 - 4ac} > 0$. But since $b > 0$, $-b - \sqrt{b^2 - 4ac} < 0$, so we must discard the $p^z_{1,0-}$ root for $a, b > 0$. As for the plus solution, note that $-b + \sqrt{b^2 - 4ac} > 0$ for all $c < 0$. Such a constraint on $c$ also ensures that the discriminant is positive. Thus, for $a, b > 0$, we must enforce that $c < 0$ and take the plus solution to Eq. (53):

$$(a > 0) \text{ and } (b > 0) \text{ and } (c < 0) \Rightarrow p^z_{1,0+}. \tag{55}$$

Suppose now that $a > 0$ and $b < 0$. For the plus solution, we require only that the discriminant be positive:

$$(a > 0) \text{ and } (b < 0) \text{ and } (b^2 - 4ac > 0) \Rightarrow p^z_{1,0+}. \tag{56}$$

As for the minus solution, we again require $-b - \sqrt{b^2 - 4ac} > 0 \Leftrightarrow 0 < b^2 - 4ac < b^2$. This is true for $c > 0$ and $b^2 - 4ac > 0$:

$$(a > 0) \text{ and } (b < 0) \text{ and } (c > 0) \text{ and } (b^2 - 4ac > 0) \Rightarrow p^z_{1,0-}. \tag{57}$$

Next, assume $a < 0$ and $b > 0$. For the plus solution, we require now that $-b + \sqrt{b^2 - 4ac} < 0$ to enforce that the plus root is positive. This is equivalent to $0 < b^2 - 4ac < b^2$, which is true for all $c < 0$ and $b^2 - 4ac > 0$ :

$$(a < 0) \text{ and } (b > 0) \text{ and } (c < 0) \text{ and } (b^2 - 4ac > 0) \Rightarrow p^z_{1,0+}. \tag{58}$$

As for the minus root, we need that $-b - \sqrt{b^2 - 4ac} < 0$. For this to be true, we require only that $b^2 - 4ac > 0$:

$$(a < 0) \text{ and } (b > 0) \text{ and } (b^2 - 4ac > 0) \Rightarrow p^z_{1,0-}. \tag{59}$$

Finally, consider $a, b < 0$. Looking at the plus solution, we require that $-b + \sqrt{b^2 - 4ac} < 0$. But this is not possible, since $+\sqrt{b^2 - 4ac}$ can never be less than a negative number. We therefore discard the plus solution. Considering the minus solution, we need $-b - \sqrt{b^2 - 4ac} < 0$. But this is true for any $c > 0$, which also ensures that the discriminant is real:

$$(a < 0) \text{ and } (b < 0) \text{ and } (c > 0) \Rightarrow p^z_{1,0-}. \tag{60}$$

We have therefore derived six conditions, Eq's (55) through (60), that tell us under which conditions to choose either the $p^z_{1,0+}$ or the $p^z_{1,0-}$ solution to the quadratic equation (49). We implement these conditions by introducing Heaviside theta functions into the expression for the cross-section:

$$\begin{aligned}
&\frac{d\sigma^{2\to 3}}{d^2\boldsymbol{p}_1 d^3k_5} \\
&\quad = \Theta[b^2-4ac] \\
&\qquad \times \big(\sigma_+(\Theta[+a]\Theta[+b]\Theta[-c]+\Theta[+a]\Theta[-b]+\Theta[-a]\Theta[+b]\Theta[-c]) \\
&\qquad + \ \sigma_-(\Theta[-a]\Theta[-b]\Theta[+c]+\Theta[-a]\Theta[+b]+\Theta[+a]\Theta[-b]\Theta[+c])\big), \qquad (61)
\end{aligned}$$

where

$$\sigma_\pm \equiv \left(\frac{(gg_Sg_A)^2}{2^4 s^3(2\pi)^5}\frac{\Theta[(k_5^z)^2]}{E_5}\frac{J^{-1}\Theta[((2-x_5)E)^2-E_1^2-E_4^2]}{E_1E_4(P^2-m_C^2)^2}\right)_{p_1^z=p^z_{1,0\pm}}. \qquad (62)$$

That is, $\sigma_\pm$ is the term in the cross-section Eq. (52) that is evaluated for $p_1^z = p^z_{1,0\pm}$, with the kinematic constraint on the energies enforced by the Heaviside theta function discussed in the paragraph preceding Eq. (50).

In order to perform our later analyses with greater ease, let us simplify Eq. (61) before we proceed. Notice that a necessary condition for three of the theta functions on the right hand side of Eq. (61) to be non-zero is that $a<0$. Using our expression for $a$ in Eq. (54), we may solve for $x_5$ when $a=0$ and probe the sign behaviour of $a$ on either side of the root. We find that

$$x_{5,a=0} = 1+\frac{\boldsymbol{k}_5^2+m_D^2}{4E^2}. \qquad (63)$$

Now, given any $\epsilon>0$, we can substitute $x_5 = x_{5,a=0}-\epsilon$ into $a$. For this value of $x_5$, $a$ evaluates to $16\epsilon E^2>0$. Next, substituting $x_5 = x_{5,a=0}+\epsilon$ into $a$ yields $a=-16\epsilon E^2<0$. Given that $a$ is linear in $x_5$, these two statements respectively tell us that to the left of $x_{5,a=0}$, $a$ is strictly positive, while to the right of $x_{5,a=0}$, $a$ is strictly negative. That is,

$$\begin{cases} a>0 \text{ for } x_5 < x_{5,a=0}, \\ a<0 \text{ else.} \end{cases} \qquad (64)$$

But since $x_{5,a=0}$ is strictly greater than 1, Eq. (64) tells us that for all $x_5<1$, $a>0$. Therefore, the three terms in Eq. (61) that contain the factor $\Theta[-a]$

never contribute to the cross-section where it has support (in the region $m_D/E < x_5 < 1$). Furthermore, in this region, $\Theta[+a] = 1$. We may therefore, in Eq. (61), elide the terms containing $\Theta[-a]$ and set $\Theta[+a] = 1$. Hence,

$$\frac{d\sigma^{2\to3}}{d^2\boldsymbol{p}_1 d^3k_5} = \Theta[b^2 - 4ac]\big(\sigma_+\Theta[+b]\Theta[-c] + \sigma_+\Theta[-b] + \sigma_-\Theta[-b]\Theta[+c]\big). \quad (65)$$

Upon inspection of Eq. (65), one can note that for the final two terms in the parentheses to contribute to the cross-section, it is necessary that $b < 0$. However, expanding our expression for coefficient $b$ in Eq. (54) in the large energy limit, we find that to leading order, $b = 16E^3(1 - x_5)x_5$. For $m_D/E < x_5 < 1$, this leading order term is strictly positive. As for the corrections to $b$ at NLO, we obtain a small but highly non-trivial expression that does not allow us to analytically rule out small negative contributions to coefficient $b$. Once more, however, our numerical investigations suggest that coefficient $b$ does not have any negative support for $m_D/E < x_5 < 1$. This leads us to conclude that for all $m_D/E < x_5 < 1$, $b > 0$. Thus,

$$\frac{d\sigma^{2\to3}}{d^2\boldsymbol{p}_1 d^3k_5} = \sigma_+\Theta[b^2 - 4ac]\Theta[-c]. \quad (66)$$

For our final simplification, recall that $a > 0$ for all $m_D/E < x_5 < 1$. Combining this with the fact that we need $c < 0$ for Eq. (66) to have support, we are guaranteed that $\Theta[b^2 - 4ac] = 1$ in the region. Hence, our expression for the differential cross-section simplifies to

$$\frac{d\sigma^{2\to3}}{d^2\boldsymbol{p}_1 d^3k_5} = \sigma_+\Theta[-c], \quad (67)$$

with $\sigma_+$ defined as in Eq. (62). We confirmed numerically (for the details on our implementation of the numerics, see the paragraph immediately preceing Fig. (5)) that the cross-section obtained from Eq. (67) is identical to cross-section obtained from the full expression in Eq. (61), suggesting that our simplifications from Eq. (61) to Eq. (67) are valid.

A natural question one might ask is how the condition that $c < 0$ in Eq. (62) further constrains the support of the differential cross-section. Once again, probing the sign behaviour of the coefficient proves to be fruitful. Since the differential cross-section is not necessarily zero when $c < 0$, but is identically zero when $c > 0$, we are interested in finding the roots of $c$ in $x_5$, and probing the sign behaviour of $c$ on either side of the roots. In

*Mathematica*, we solve for $x_5$ when $c = 0$, and expand each root in the large energy limit. To leading order, we find that $c$ vanishes when

$$x_5 \equiv x_{5,c=0\pm} = 1 \pm \frac{\sqrt{\boldsymbol{p}_1^2 + m_C^2}}{2E}. \tag{68}$$

Following a process analogous to that described in the paragraph immediately preceding Eq. (64) in which we probe the sign behaviour of coefficient $a$, we find for coefficient $c$ that

$$\begin{cases} c > 0 \text{ for } 1 - \frac{\sqrt{\boldsymbol{p}_1^2+m_C^2}}{2E} < x_5 < 1 + \frac{\sqrt{\boldsymbol{p}_1^2+m_C^2}}{2E}, \\ c < 0 \text{ else.} \end{cases} \tag{69}$$

But given that our differential cross-section only has support in the region $m_D/E < x_5 < 1$, we are not interested in the sign behaviour of $c$ outside this region. Hence, within the region $m_D/E < x_5 < 1$,

$$\begin{cases} c > 0 \text{ for } 1 - \frac{\sqrt{\boldsymbol{p}_1^2+m_C^2}}{2E} < x_5 < 1, \\ c < 0 \text{ for } \frac{m_D}{E} < x_5 < 1 - \frac{\sqrt{\boldsymbol{p}_1^2+m_C^2}}{2E}. \end{cases} \tag{70}$$

Given Eq. (70) and that $c < 0$ is necessary for non-zero contributions to the differential cross-section, we arrive at tighter bounds than our previously found region of support $m_D/E < x_5 < 1$. We see that, to the left of $x_{5,c=0-}$, $c < 0$, and that $c$ changes sign to the right of $x_{5,c=0-}$. Thus, to the right of $x_{5,c=0-}$, $\Theta[-c] = 0$. So, by Eq. (67), the differential cross-section vanishes for all $x_5 > x_{5,c=0-}$. We conclude that the differential cross-section has support only in the region

$$\frac{m_D}{E} < x_5 < 1 - \frac{\sqrt{\boldsymbol{p}_1^2 + m_C^2}}{2E}. \tag{71}$$

In the small $\boldsymbol{p}_1$ limit, the upper bound on $x_5$ in Eq. (71) reduces to $x_5 = 1 - m_C/2E$. Our numerics show that the $x_5$ limit is reached at $1 - m_C/2E$, consistent with our analytics.

Finally, one obtains the differential cross-section for the $2 \to 3$ case by

integrating over $\boldsymbol{p}_1$ and $\boldsymbol{k}_5$:

$$\begin{aligned}\frac{d\sigma^{2\to3}}{dx_5} &= \int d^2\boldsymbol{p}_1 d^2\boldsymbol{k}_5 \frac{d\sigma^{2\to3}}{d^2\boldsymbol{p}_1 d^2\boldsymbol{k}_5 dx_5} \\ &= \int_0^{2\pi} d\theta \int_0^{|\boldsymbol{p}_1|_{\max}} d|\boldsymbol{p}_1||\boldsymbol{p}_1| \int_0^{2\pi} dt \int_0^{|\boldsymbol{k}_5|_{\max}} d|\boldsymbol{k}_5||\boldsymbol{k}_5| \\ &\quad \times \frac{d\sigma^{2\to3}}{d^2\boldsymbol{p}_1 d^2\boldsymbol{k}_5 dx_5} \\ &= 2\pi \int_0^{|\boldsymbol{p}_1|_{\max}} d|\boldsymbol{p}_1| \int_0^{2\pi} dt \int_0^{|\boldsymbol{k}_5|_{\max}} d|\boldsymbol{k}_5||\boldsymbol{p}_1||\boldsymbol{k}_5| \frac{d\sigma^{2\to3}}{d^2\boldsymbol{p}_1 d^2\boldsymbol{k}_5 dx_5}. \end{aligned} \tag{72}$$

We choose to take $\boldsymbol{p}_1$ parallel to the $z$-axis to make the $\theta$-integral trivial.

We may now calculate the conditional probability distribution

$$\frac{1}{\sigma^{2\to2}} \frac{d\sigma^{2\to3}}{dx_5}, \tag{73}$$

where $\sigma^{2\to2}$ given in Eq. (33) is the total cross-section for the $2 \to 2$ scattering process described by Fig. (3), and $d\sigma^{2\to3}/dx_5$ is the differential cross-section for the emission of a scalar particle, as given in Eq. (72).

The integrations in the expression for $d\sigma^{2\to3}/dx_5$ were performed numerically in *Mathematica*, taking for the energy $E = 10$ GeV, the mass of the $C$ field $m_C = 100$ MeV, the mass of the $D$ field $m_D = 100$ MeV, and the coupling constant $g_S = 0.3$. As for the bounds on the integrals, recall that we choose that $\boldsymbol{p}_1$ have only a small deviation from the $z$-axis, $|\boldsymbol{p}_1|_{\max} = \xi E$, for $\xi \ll 1$. We plot curves for four different values of $\xi$, starting from $\xi = 0.05$ up to $\xi = 0.20$ in increments of 0.05. Finally, from the Heaviside theta function $\Theta((k_5^z)^2) = \Theta((x_5 E)^2 - \boldsymbol{k}_5^2 - m_D^2)$, we obtain an upper bound on $\boldsymbol{k}_5$ given by $|\boldsymbol{k}_5|_{\max} = ((x_5 E)^2 - m_D^2)^{1/2}$. The conditional probability distribution in Eq. (73) is plotted in Fig. 5 below, as a function of $x_5$.

## 6. Discussion

We first note that our distributions in Fig. (5) have enlargement at large-$x_5$, in contrast with particle emission in a gauge theory where one has enlargement at small-$x$ due to the higher weight from the polarization vectors in the small-$x$ region. We understand the enlargement of our distributions at large-$x_5$ to

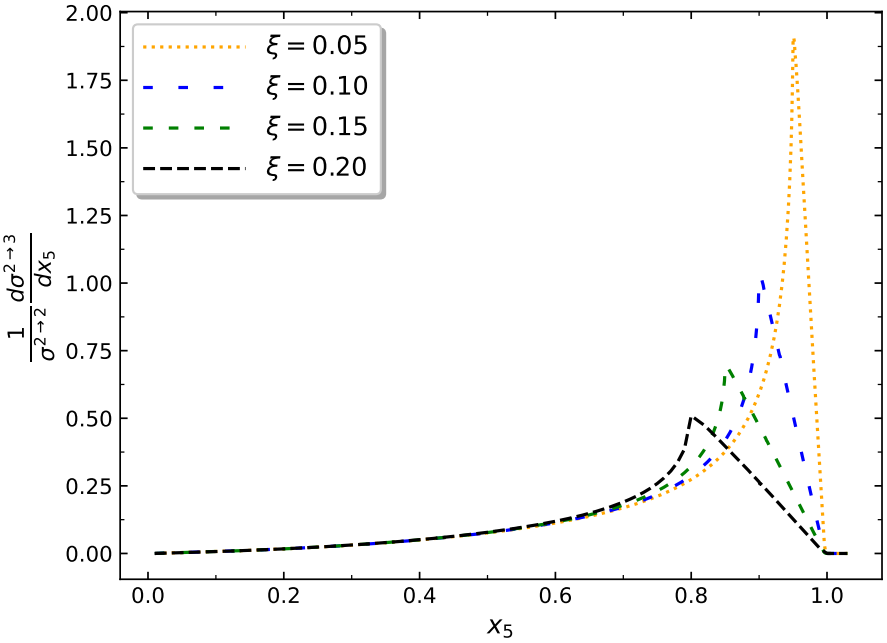


Figure 5: Conditional probability distributions for the emission of a single scalar particle in our model of radiative emissions, plotted for various values of $\xi$, where $\xi$ controls the maximum perpendicular component of the emitting particle: $|\boldsymbol{p}_1|_{\max} = \xi E$.

be a result of the following. One can show that

$$\frac{d\sigma^{2\to 3}}{dx_5 d^2\boldsymbol{k}_5 d^2\boldsymbol{p}_1} \sim \frac{1}{(\boldsymbol{k}_5 - \boldsymbol{p}_1)^4} \tag{74}$$

for $x_5 \to 1$. This tells us that the differential cross-section can become singular as $x_5 \to 1$, so an enhancement of our distributions as $x_5 \to 1$ is not unexpected. This feature of our theory permits a higher sensitivity to the behaviour of the distributions near the kinematic cut-off at $x_5 = 1$.

The rapid growth of the distributions in Fig. (5) at large-$x_5$ indicate that the matrix element squared grows rapidly as we approach the kinematic bound of $x_5 = 1$. However, one observes a smooth squeezing of the distributions in Fig. (5) to zero as $x_5 \to 1$; our distributions that were obtained by enforcing exact, finite kinematics obey energy conservation.

One may also observe that the peak of the curves in Fig. (5) move to the left (i.e., towards smaller $x_5$ values) as $\xi$ increases, and the downward slope to the right of the peak decreases. We understand this to be a result of the decrease in available phase space resulting from the kinematic limit that $c < 0$ being realized at large $x_5$. Recalling our expression for the upper bound on $x_5$,

$$x_5 < 1 - \frac{\sqrt{\boldsymbol{p}_1^2 + m_C^2}}{2E}, \tag{75}$$

one notes that for larger values of $\xi$, this limit is hit earlier because $\boldsymbol{p}_1$ gets larger with $\xi$. We confirmed this numerically. By modifying the $c$ condition to allow for

$$x_5 < 1 - \alpha\frac{\sqrt{\boldsymbol{p}_1^2 + m_C^2}}{2E}, \tag{76}$$

where $\alpha$ was varied from 1/2 to 2, we saw that for smaller values of $\alpha$ the peaks were shifted to the right (i.e., towards larger $x_5$ values), while for larger $\alpha$, the peaks were shifted to the left. This confirms that the $x_5$ value of the peaks of the curves is controlled by the value of $\xi$. As $\xi$ increases, the kinematic limit on $c$ is realized for smaller values of $x_5$, resulting in the peaks moving to the left and the downward slope decreasing.

We would like to get a sense of the extent to which our differential cross-section $d\sigma^{2\to 3}/dx_5$ depends on our treatment of the kinematics. That is, how much is $d\sigma^{2\to 3}/dx_5$ modified by an exact treatment of the finite kinematics, in comparison to a more naïve approach to dealing with the kinematic constraints? In the usual treatment of energy loss due to radiative emissions

in QCD, one enforces the kinematic constraints *a posteriori*; nowhere in the calculation does one enforce the kinematics by integrating over some energy-momentum conserving Dirac delta function. This is in contrast to the calculation we performed in Sec. 5, where we took great care to rigorously treat the exact, finite kinematics throughout the calculation.

In order to get a sense of the modification of our distributions in Fig. (6) following a more naïve approach to treating the kinematics, we note that our treatment of the energy-momentum conserving Dirac delta function in Eq. (41) lead us to constrain the available phase space by introducing a number of Heaviside theta functions. Hence, in order to lift the kinematic constraints imposed by the energy-momentum conserving Dirac delta function, we simply elide the Heaviside theta functions in our expression for the differential cross-section in Eq. (72). One result of such an omission is that the upper bound on our integration over $|\boldsymbol{k}_5|$ is no longer well-defined. In order to deal with this, and to better make contact with the usual *a posteriori* treatment of the kinematics, we choose to limit the $|\boldsymbol{k}_5|$ phase space in the usual way, by imposing a finite $|\boldsymbol{k}_{5,\text{max}}| = x_5 E$.

In the following, we frequently refer to the naïve and the exact distribution(s); for clarity, we mean by the naïve distribution the distribution we obtain by eliding the Heaviside theta functions in Eq. (72) and imposing $|\boldsymbol{k}_{5,\text{max}}| = x_5 E$ on the integration over $|\boldsymbol{k}_5|$. We call the exact distribution the quantity we obtained in Eq. (72) and initially plotted in Fig. (5).

In Fig. (6), we plot on the same set of axes the naïve and exact conditional probability distributions for $\xi = 0.05$. Interestingly, the naïve and exact distributions are nearly identical for all $x_5$. In Fig. (6), we plot the ratio of the exact distribution to the naïve distribution. We see in Fig. (6) that this ratio is unity for nearly the entire $x_5$ range, further demonstrating the strong agreement between the naïve and exact distributions. Where the naïve and exact distributions begin to deviate from one another is the region in which $x_5$ becomes large. Indeed, one observes that the distributions seem to become distinct at the value of $x_5$ where the exact distribution starts to be suppressed due to the phase space restriction provided by the kinematic limit on the coefficient $c$. Our numerics suggest that this critical value of $x_5$ is approximately 0.95 for the choice $\xi = 0.05$, but we do not have an analytical understanding of why the naïve distribution begins to behave pathologically beyond this particular value of $x_5$.

We do however understand the pathological behaviour of the naïve distribution at large-$x_5$ to be a result of the abundant square roots in our expression

for the differential cross-section, Eq. (72). Since we remove the Heaviside theta functions from Eq. (72) to obtain the naïve distribution, we are no longer enforcing that the square roots be real. As a result, the square roots become imaginary at large-$x_5$, so the naïve distribution picks up a non-zero imaginary part and for some values of $x_5$, a negative real part (this is not shown in Fig. (6) or Fig. (7)).

One also notes that the naïve distribution in Fig. (6) is not identically zero beyond the kinematic limit of $x_5 = 1$; there is some non-zero support in the region $x_5 \geq 1$ before the naïve distribution eventually goes to zero. This is to be contrasted with the exact distribution in Fig. (6), which is identically zero in the region $x_5 \geq 1$. Hence, our exact distribution respects energy conservation, while our naïve distribution does not in general respect conservation of energy.

## 7. Conclusions

We computed in Eq. (14) the multiplicity distribution for the vacuum emission of a single inclusive soft and collinear gluon using the usual methods of radiative energy loss in QCD. As expected from following the usual *a posteriori* treatment of the kinematics, we obtained a distribution in Fig. (2) that does not in general respect conservation of energy. In particular, the amplitude yields a probability with support out to $x \to \infty$. When we impose the restriction that the hard emitting parton continue moving in the forward direction, then only does the distribution get cut-off at a physically reasonable $x_{\text{max}} < 1$.

We then introduced a scalar model of gluon bremsstrahlung (Eq. (16) to Eq. (18)) in order to rigorously probe the effects of exact, finite kinematics in a fully solved (to leading order) calculation. Within the framework of this simplified model of radiative emissions, we computed in Eq. (33) the total $2 \to 2$ cross-section as a primer for the $2 \to 3$ differential cross-section calculation, and to eventually divide out the $2 \to 3$ differential cross-section with the $2 \to 2$ cross-section to make better contact with the usual single inclusive gluon distribution calculation. Naturally, in computing the $2 \to 2$ cross-section, we integrated over the energy-momentum conserving Dirac delta function and obtained kinematic limits on the products of the interaction. That is, we obtained constraints on the momenta $p_4$ and $p_1$ of the parent particle and the away-side particle, respectively. These kinematics limits proved to be relatively simple to implement. In particular, we found that the

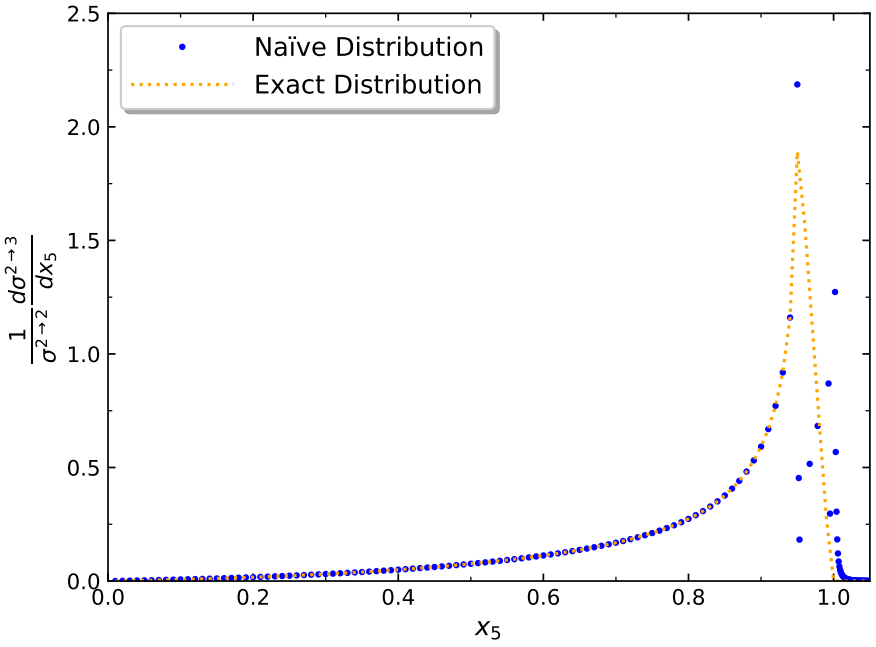


Figure 6: Naïve and exact conditional probability distributions for the emission of a single particle in our scalar model of radiative emissions, taking $\xi = 0.05$. The naïve distribution was obtained in analogy to the usual *a posterori* treatment of the kinematics in the QCD energy loss formalism, while the exact distribution was computed by enforcing the exact, finite kinematics throughout the calculation.

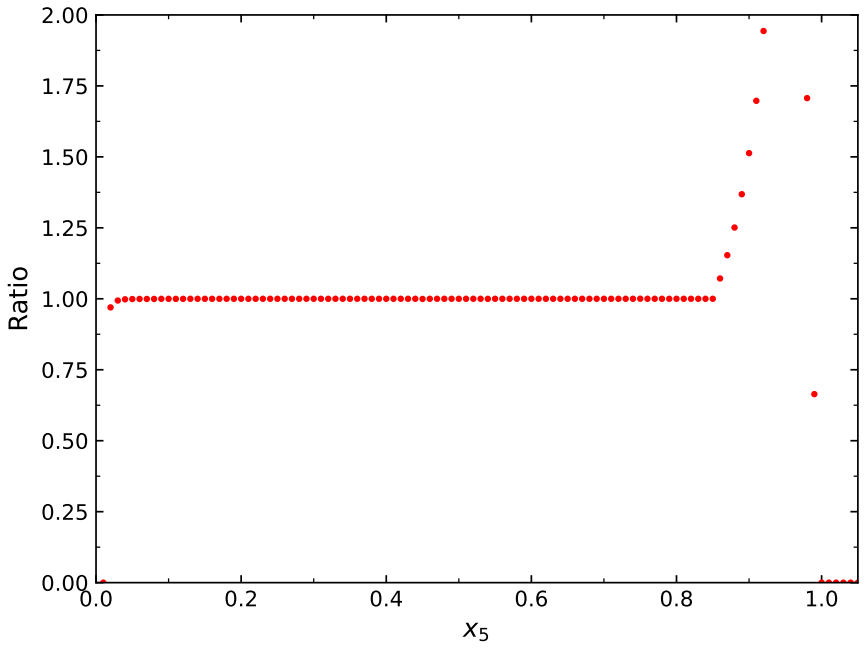


Figure 7: A plot showing the ratio between the exact and naïve conditional probability distributions for the emission of a single particle in our scalar model of radiative emissions.

outgoing particles must be back-to-back so as to conserve the vanishing initial spatial momentum, and that the magnitude of the perpendicular component of the momentum of particle $C$ be less than some number $E(1 - m_C^2/(4E^2))$, where $E$ is the energy of each of the incoming particles, and $m_C$ is the mass of particle $C$. Since we assume that $m_C \ll E$, and that the emitting particle be constrained within some small cone around the $z$-axis, $|\boldsymbol{p}_1|_{\max} \equiv \xi E$, where $\xi \ll 1$ is some real number, the constraint on the perpendicular component of particle $C$ is satisfied by assumption.

Next, we computed the differential cross-section $d\sigma^{2\to3}/dx_5$ in Eq. (72) for the emission of a scalar particle in our model of radiative emissions. By the requirement that the emitted particle have at least enough energy to come on mass-shell, we obtained a lower bound on the energy of the emitted particle, namely that $x_5 \geq m_D/E$, where $m_D$ is the mass of the emitted particle. This is identical to the small-$x$ kinematic constraint in the usual QCD-based energy loss framework, in which one invokes some IR scale $\sim \mu$ and sets $x_{\min} = \mu/E$.

The remainder of the kinematic limits, as obtained from integration over the energy-momentum conserving Dirac delta function, were significantly more complicated than the $2 \to 2$ case, as we note in the following.

In finding the roots of the argument of the energy-conserving Dirac delta function, we were required to introduce a factor $\Theta[((2-x_5)E)^2 - E_1^2 - E_4^2]$ to ensure that we preserved the overall sign of the equation; this was necessary because we squared both sides of the equation for the roots of the argument of the energy-conserving Dirac delta function, introducing a sign ambiguity. $E_1$ is the energy of the emitting particle $C$ and $E_4$ is the energy of the away-side particle $B$. Both our analytical and numerical investigation of the argument of this Heaviside theta function informs us that the Heaviside theta function has support only for $x_5 < 1$. When combined with our lower bound on $x_5$, the restriction $x_5 < 1$ means that our differential cross-section for the $2 \to 3$ case has support strictly in the region $m_D/E < x_5 < 1$.

Continuing with evaluating the energy conserving Dirac delta function, we were required to solve a quadratic polynomial in $p_1^z$. Our approach was to use the usual quadratic formula with coefficients $a, b$ and $c$, but to enforce that the discriminant was constrained to always be positive (so that the two solutions $p_{1,0\pm}^z$ be real), and that the two solutions are positive. We enforced these two constraints by considering cases for the signs of the coefficients $a, b$ and $c$. We obtained six conditions, Eq's (55) through (60), that tell us under which conditions to choose either the $p_{1,0+}^z$ or the $p_{1,0-}^z$ solution to the quadratic equation, and these conditions on the signs of the coefficients were enforced by introducing Heaviside theta functions into our expression for the differential cross-section, as in Eq. (61). However, by studying the sign behaviour of the coefficients, we were able to simplify these six conditions down to a single condition, namely that we require $c < 0$ for the differential cross-section to have support, as in Eq. (67). We then found the roots of coefficient $c$ in $x_5$, and were able to further improve our previously found bounds on the differential cross-section in terms of $x_5$ by noting that $c < 0$ for

$$\frac{m_D}{E} < x_5 < 1 - \frac{\sqrt{\boldsymbol{p}_1^2 + m_C^2}}{2E}, \tag{77}$$

which we derived in Eq. (71). That is, our differential cross-section for the emission of a single scalar particle has support strictly within the region in Eq. (77). In the small $\boldsymbol{p}_1$ limit, the upper bound on $x_5$ in Eq. (77) becomes $1 - m_C/(2E)$, which is in good agreement with the upper bound shown by the numerics. Once again, the lower bound of Eq. (77) is identical to the minimum

value of $x_5$ used in sophisticated energy-loss models, while we note that the upper bound of Eq. (77) is strictly less than 1, which is to say our distribution does not violate conservation of energy. This is to be contrased with the usual distribution obtained by an *a posterori* treatment of the kinematics, as in Fig. (2).

Next, we plotted in Fig. (5) the conditional probability distribution

$$\frac{1}{\sigma^{2\to 2}}\frac{d\sigma^{2\to 3}}{dx_5} \tag{78}$$

for the emission of a scalar particle in our model of radiative emissions, for various values of $\xi$, where $|\boldsymbol{p}_1|_{\max} = \xi E$ controls the maximum perpendicular component of the emitting particle. We noted that our distributions in Fig. (5) displayed an enlargement at large $x_5$, in contrast with particle emission in a gauge theory. We understand the enhancement at large $x_5$ of our distributions in Fig. (5) to be a result of the form of our differential cross-section in the large-$x_5$ region, as shown in Eq. (74). In particular, as $\boldsymbol{k}_5$ and $\boldsymbol{p}_1$ become collinear in the limit $x_5 \to 1$, the differential cross-section becomes singular. Despite of the enlargement of our distributions, in Fig. (5) one clearly notes that the distributions all identically vanish in the kinematically forbidden region of $x_5 > 1$. This suggests that a rigorous treatment of the exact, finite kinematics yields a differential cross-section that respects energy conservation, as it must. This is in contrast with the usual *a posteriori* treatment of the kinematics, in which one encounters a violation of energy conservation.

Another feature of the distributions in Fig. (5) is that the peak of the curves shift toward smaller $x_5$ values as we increase $\xi$, as well as the downward slope to the right of the peak decreasing as $\xi$ increases. We reasoned that this was the result of the upper bound of $x_5$ becoming smaller as $\boldsymbol{p}_1$ became larger; as $\xi$ increases, so does the allowed maximum value of $|\boldsymbol{p}_1|$, which results in the upper bound $1 - \sqrt{\boldsymbol{p}_1^2 + m_C^2}/(2E)$ on $x_5$ to be realized for smaller values of $x_5$, resulting in the peaks moving to the left and the downward slope decreasing.

Finally, we probed the extent to which our differential cross-section $d\sigma^{2\to 3}/dx$ depends on our treatment of the kinematics. In particuar, we compared our distributions in Fig. (5) to the distributions one obtains by following a more naïve approach to the kinematics, similar to the usual *a posteriori* treatment in the QCD regime. In order to obtain these "naïve distributions," we lifted the kinematic constraints of our distributons in Fig. (5) by eliding the Heaviside theta functions that were previously used to enforce the kinematic constraints, and took $|\boldsymbol{k}_5|_{\max} = x_5 E$, as one does in the usual *a*

*posteriori* treatment of the kinematics. The resulting distribution for $\xi = 0.05$ is shown in Fig. (6), on the same set of axes as the exact distribution for $\xi = 0.05$. We noted that the two distributions in Fig. (6) are nearly identical for all $x_5$, with the clear exception being the large-$x_5$ region, in which the exact distribution smoothly squeezes to zero, while the naïve distribution behaves pathologically before going to zero *beyond* the strict kinematic limit of $x_5 = 1$. We attribute the pathological behaviour of the naïve distribution to our removal of the Heaviside theta functions that previously prevented a number of square roots from becoming imaginary. In the naïve distribution, these Heaviside theta functions are not present, and so these square roots can become imaginary. This can cause the distribution to become imaginary with a potentially negative real part due to the imaginary square roots multiplying each other.

We plot in Fig. (7) the ratio between the naïve and exact distributions, and see that the ratio is nearly unity for the entire $x_5$ range, until the distributions deviate from one another in the large-$x_5$ region. In fact, we note that the naïve and exact distributions begin to deviate from one another at the value of $x_5$ where the exact distribution begins to be suppressed by the restriction of the phase space provided by the kinematic limit on coefficient $c$.


### 8. Acknowledgments

The authors wish to thank the SA-CERN Collaboration and the National Institute for Theoretical and Computational Sciences (NITheCS) for their generous support. The authors also wish to thank Matthew Sievert for valuable discussions.


# Appendices

### A. Conventions

Throughout this thesis, we use the mostly minus metric

$$\eta = \text{diag}(1, -1, -1, -1), \tag{79}$$

and take

$$\hbar = c = 1. \tag{80}$$

The colour factor

$$C_R = \frac{N^2-1}{2N} = 4/3 \tag{81}$$

for QCD. As for our coordinate definitions, we take a four-vector to be not bold-faced, e.g. $p$ and $k$. A three-vector is taken to be bold-faced with an arrow, e.g. $\vec{\boldsymbol{p}}$ and $\vec{\boldsymbol{k}}$. A transverse two-vector is taken to be bold-faced but without an arrow, e.g. $\boldsymbol{p}$ and $\boldsymbol{k}$. We use the non-symmetrized convention for our lightcone coordinates,

$$\begin{aligned} p^+ &= p^0 + p^3, \\ p^- &= p^0 - p^3, \\ \boldsymbol{p} &= \boldsymbol{p}. \end{aligned} \tag{82}$$

### B. Component-wise, $(1/E)\not{\epsilon}\not{k} \ll (1/E)\not{\epsilon}\not{p}$

In the following, we will argue that every component of the matrix $(1/E)\not{\epsilon}\not{k}$ is of higher order than the corresponding components of $(1/E)\not{\epsilon}\not{p}$, and may therefore be neglected in favour of contributions to the matrix element from the latter matrix. Using our assumed kinematics in Eq. (1), one may readily compute the matrices $\not{p}$, $\not{k}$ and $\not{\epsilon}$, where we take the gamma matrices to be in the Dirac representation. We find that

$$\begin{aligned}
\not{p} &\simeq \begin{pmatrix} E(1-x) & 0 & -E(1-x) & k^1 - ik^2 \\ 0 & E(1-x) & k^1 + ik^2 & E(1-x) \\ E(1-x) & -k^1 + ik^2 & -E(1-x) & 0 \\ -k^1 - ik^2 & -E(1-x) & 0 & -E(1-x) \end{pmatrix}, \\
\not{k} &\simeq \begin{pmatrix} xE & 0 & -xE & -k^1 + ik^2 \\ 0 & xE & -k^1 - ik^2 & xE \\ xE & k^1 - ik^2 & -xE & 0 \\ k^1 + ik^2 & -xE & 0 & -xE \end{pmatrix}, \\
\not{\epsilon} &\simeq \begin{pmatrix} \frac{\boldsymbol{k}\cdot\boldsymbol{\epsilon}}{2xE} & 0 & \frac{\boldsymbol{k}\cdot\boldsymbol{\epsilon}}{2xE} & -\epsilon^1 + i\epsilon^2 \\ 0 & \frac{\boldsymbol{k}\cdot\boldsymbol{\epsilon}}{2xE} & -\epsilon^1 - i\epsilon^2 & -\frac{\boldsymbol{k}\cdot\boldsymbol{\epsilon}}{2E} \\ -\frac{\boldsymbol{k}\cdot\boldsymbol{\epsilon}}{2xE} & \epsilon^1 - i\epsilon^2 & -\frac{\boldsymbol{k}\cdot\boldsymbol{\epsilon}}{2xE} & 0 \\ \epsilon^1 + i\epsilon^2 & \frac{\boldsymbol{k}\cdot\boldsymbol{\epsilon}}{2xE} & 0 & -\frac{\boldsymbol{k}\cdot\boldsymbol{\epsilon}}{2xE} \end{pmatrix}.
\end{aligned} \tag{83}$$

In order to compute $\not{p}$, we used the high energy and softness assumptions to write $\sqrt{(1-x)^2E^2 - \boldsymbol{k}^2} \simeq (1-x)E$. Using collinearity, we get that

$\sqrt{(xE)^2 - \boldsymbol{k}^2} \simeq xE$, a fact we used to compute $\not{k}$. To compute $\not{\epsilon}$, we simply evaluated the contraction $\gamma_\mu \epsilon^\mu$.

The products $\not{\epsilon}\not{p}$ and $\not{\epsilon}\not{k}$ may then be computed. One finds that the components of the first column of $(1/E)\not{\epsilon}\not{p}$ are given by

$$\begin{aligned}
\left(\frac{1}{E}\not{\epsilon}\not{p}\right)_{11} &= \frac{\boldsymbol{k}\cdot\boldsymbol{\epsilon}}{xE} - \frac{\boldsymbol{k}\cdot\boldsymbol{\epsilon}}{E} + \frac{(\epsilon^1 - i\epsilon^2)\,(k^1 + ik^2)}{E} \\
\left(\frac{1}{E}\not{\epsilon}\not{p}\right)_{21} &= \frac{(k^1 + ik^2)\,\boldsymbol{k}\cdot\boldsymbol{\epsilon}}{2E^2 x} + (x-1)\left(\epsilon^1 + i\epsilon^2\right) \\
\left(\frac{1}{E}\not{\epsilon}\not{p}\right)_{31} &= \frac{\boldsymbol{k}\cdot\boldsymbol{\epsilon}}{E} - \frac{\boldsymbol{k}\cdot\boldsymbol{\epsilon}}{xE} \\
\left(\frac{1}{E}\not{\epsilon}\not{p}\right)_{41} &= \frac{(k^1 + ik^2)\,\boldsymbol{k}\cdot\boldsymbol{\epsilon}}{2E^2 x} - (x-1)\left(\epsilon^1 + i\epsilon^2\right),
\end{aligned} \tag{84}$$

and the first column of $(1/E)\not{\epsilon}\not{k}$ has components

$$\begin{aligned}
\left(\frac{1}{E}\not{\epsilon}\not{k}\right)_{11} &= \frac{\boldsymbol{k}\cdot\boldsymbol{\epsilon}}{E} - \frac{(\epsilon^1 - i\epsilon^2)\,(k^1 + ik^2)}{E} \\
\left(\frac{1}{E}\not{\epsilon}\not{k}\right)_{21} &= -\left(\frac{(k^1 + ik^2)\,\boldsymbol{k}\cdot\boldsymbol{\epsilon}}{2E^2 x} + x\left(\epsilon^1 + i\epsilon^2\right)\right) \\
\left(\frac{1}{E}\not{\epsilon}\not{k}\right)_{31} &= -\frac{\boldsymbol{k}\cdot\boldsymbol{\epsilon}}{E} \\
\left(\frac{1}{E}\not{\epsilon}\not{k}\right)_{41} &= -\left(\frac{(k^1 + ik^2)\,\boldsymbol{k}\cdot\boldsymbol{\epsilon}}{2E^2 x} - x\left(\epsilon^1 + i\epsilon^2\right)\right).
\end{aligned} \tag{85}$$

Let us go through each of these components, and show that $((1/E)\not{\epsilon}\not{p})_{ij} \gg ((1/E)\not{\epsilon}\not{k})_{ij}$ for $i \in \{1,2,3,4\}$ and $j = 1$. One may follow a similar process to see that $((1/E)\not{\epsilon}\not{p})_{ij} \gg ((1/E)\not{\epsilon}\not{k})_{ij}$ for all $i, j \in \{1,2,3,4\}$. For $(i,j) = (1,1)$, softness gives

$$\frac{\boldsymbol{k}\cdot\boldsymbol{\epsilon}}{xE} \gg \frac{\boldsymbol{k}\cdot\boldsymbol{\epsilon}}{E}, \tag{86}$$

and, since the final term in $((1/E)\not{\epsilon}\not{p})_{11}$ is of the same order as the term on the right-hand side of Eq. (86), it follows that $((1/E)\not{\epsilon}\not{p})_{11} \gg ((1/E)\not{\epsilon}\not{k})_{11}$. As for components $(i,j) = (2,1)$, note that

$$\left(\frac{1}{E}\not{\epsilon}\not{p}\right)_{21} = -\left(\frac{1}{E}\not{\epsilon}\not{k}\right)_{21} - (\epsilon^1 + i\epsilon^2). \tag{87}$$

Looking at each term in $((1/E)\not{\epsilon}\not{k})_{21}$, we see that

$$\frac{(k^1 + ik^2)\,\boldsymbol{k}\cdot\boldsymbol{\epsilon}}{2E^2x} \sim \frac{\boldsymbol{k}^2}{E^2x} = x\left(\frac{\boldsymbol{k}}{xE}\right)^2 \ll 1 \tag{88}$$

by softness and collinearity. As for the final term in $((1/E)\not{\epsilon}\not{k})_{21}$, since $x \ll 1$, contributions from $x\,(\epsilon^1 + i\epsilon^2)$ are very small. Hence, the term $(\epsilon^1 + i\epsilon^2)$ in $((1/E)\not{\epsilon}\not{p})_{21}$ is much larger than $((1/E)\not{\epsilon}\not{k})_{21}$. Hence, $((1/E)\not{\epsilon}\not{p})_{21} \gg ((1/E)\not{\epsilon}\not{k})_{21}$. Consider now components $(i,j) = (3,1)$. As with component $(i,j) = (1,1)$, softness greatly enhances the term that goes like $1/x$, and so $((1/E)\not{\epsilon}\not{p})_{31} \gg ((1/E)\not{\epsilon}\not{k})_{31}$. Finally, the argument for $(i,j) = (4,1)$ is very similar to the argument for $(i,j) = (2,1)$, and we similarly conclude that $((1/E)\not{\epsilon}\not{p})_{41} \gg ((1/E)\not{\epsilon}\not{k})_{41}$.

Therefore, $((1/E)\not{\epsilon}\not{p})_{ij} \gg ((1/E)\not{\epsilon}\not{k})_{ij}$ for $i \in \{1,2,3,4\}$ and $j = 1$, as we wanted to show. A similar analysis of the remaining components of the matrices $(1/E)\not{\epsilon}\not{p}$ and $(1/E)\not{\epsilon}\not{k}$ leads us to conclude that $((1/E)\not{\epsilon}\not{p})_{ij} \gg ((1/E)\not{\epsilon}\not{k})_{ij}$ for all $i,j \in \{1,2,3,4\}$. In conclusion, we may neglect contributions to the matrix element from $(1/E)\not{\epsilon}\not{k}$, since every component of the matrix $(1/E)\not{\epsilon}\not{p}$ is much larger than the corresponding component of $(1/E)\not{\epsilon}\not{k}$.

## C. Average over initial and sum over final states

We wish to compute the average over initial and sum over final states of the amplitude squared for single inclusive soft and collinear vacuum radiation in QCD, as described in Sec. 2.

In Eq. (6), we wrote down the amplitude to leading order in the strong coupling $g$,

$$i\mathcal{M} = \bar{u}(p)\big(i\,g\,t^a \not{\epsilon}^{a*}(k)\big)\frac{i(\not{p}+\not{k})}{P^2}\mathcal{M}_0(P,P_0)u(P_0)\cdots \tag{89}$$

Let us make clear the index structure of the right-hand side of Eq. (89):

$$i\mathcal{M} = \frac{-g}{P^2}\bar{u}^{s_p c_p j\alpha}(p)t^a_{jl}\not{\epsilon}^{*a\lambda c_\epsilon}_{\alpha\beta}(k)(\not{p}+\not{k})^{\beta\gamma}\left(\mathcal{M}_0\right)_{\gamma\omega\rho\cdots}u^{s_0 c_0 l\omega}(P_0)(\cdots)^{\rho\cdots}, \tag{90}$$

where $s_p = \pm 1/2$ and $c_p \in \{1,2,3\}$ are respectively the spin and colour of the outgoing quark, $j,l \in \{1,2,3\}$ are colour space indices, $\lambda \in \{1,2\}$ and $c_\epsilon \in \{1,2,\cdots,8\}$ are respectively the polarization and colour of the outgoing gluon, and finally $s_0 = \pm 1/2$ and $c_0 \in \{1,2,3\}$ are respectively the spin and colour of the incoming quark.

Now, recall that $\not{\epsilon}^*\not{p} = 2p\cdot\epsilon^* - \not{p}\not{\epsilon}^*$ where the final term on the right-hand side vanishes by the Dirac equation. Therefore,

$$\not{\epsilon}^{*a\lambda c_\epsilon}_{\alpha\beta}(k)\not{p}^{\beta\gamma} = 2p\cdot\epsilon^{*a\lambda c_\epsilon}(k)\delta^\gamma_\alpha. \tag{91}$$

Substituting Eq. (91) into Eq. (90), we have that

$$\begin{aligned} i\mathcal{M} &\simeq \frac{-g}{P^2}\bar{u}^{s_p c_p j\alpha}(p)t^a_{jl}(2p\cdot\epsilon^{*a\lambda c_\epsilon}(k)\delta^\gamma_\alpha)\left(\mathcal{M}_0\right)_{\gamma\omega\rho\cdots}u^{s_0 c_0 l\omega}(P_0)(\cdots)^{\rho\cdots} \\ &= \frac{-2g}{P^2}p\cdot\epsilon^{*a\lambda c_\epsilon}(k)\bar{u}^{s_p c_p j\alpha}(p)t^a_{jl}\left(\mathcal{M}_0\right)_{\alpha\omega\rho\cdots}u^{s_0 c_0 l\omega}(P_0)(\cdots)^{\rho\cdots}, \end{aligned} \tag{92}$$

where in the first line we drop the $\not{k}$ containing term as justified in Sec. B.

Let us now evaluate the dot products in Eq. (92). $P^2 = (p+k)^2 = 2p\cdot k$

by the on-shell condition. Using the definition of $p$ and $k$ in Eq. (1),

$$
\begin{aligned}
p\cdot k &= x(1-x)E^2 - \left((1-x)E\sqrt{1-\frac{\boldsymbol{k}^2}{(1-x)^2E^2}}\right)\left(xE\sqrt{1-\frac{\boldsymbol{k}^2}{(xE)^2}}\right)+\boldsymbol{k}^2\\
&= x(1-x)E^2 - x(1-x)E^2\left(1-\frac{\boldsymbol{k}^2}{2(1-x)^2E^2}+\mathcal{O}\left[\left(\frac{\boldsymbol{k}}{(1-x)E}\right)^4\right]\right)\\
&\quad\times\left(1-\frac{\boldsymbol{k}^2}{2(xE)^2}+\mathcal{O}\left[\left(\frac{\boldsymbol{k}}{xE}\right)^4\right]\right)+\boldsymbol{k}^2\\
&= x(1-x)E^2 - x(1-x)E^2\Bigg(1+\frac{\boldsymbol{k}^4}{4x^2(1-x)^2E^4}-\frac{\boldsymbol{k}^2}{2(xE)^2}\\
&\quad-\frac{\boldsymbol{k}^2}{2(1-x)^2E^2}+\mathcal{O}\Bigg[\left(\frac{\boldsymbol{k}}{xE}\right)^4,\frac{\boldsymbol{k}^6}{x^4E^6(1-x)^2},\left(\frac{\boldsymbol{k}}{(1-x)E}\right)^4,\\
&\qquad\frac{\boldsymbol{k}^6}{x^2(1-x)^4E^6},\left(\frac{\boldsymbol{k}}{x(1-x)E^2}\right)^8\Bigg]\Bigg)+\boldsymbol{k}^2\\
&= -\frac{\boldsymbol{k}^4}{4x(1-x)E^2}+\frac{\boldsymbol{k}^2}{2x}(1-x)+\frac{\boldsymbol{k}^2}{2(1-x)}x\\
&\quad-x(1-x)E^2\mathcal{O}\Bigg[\left(\frac{\boldsymbol{k}}{xE}\right)^4,\frac{\boldsymbol{k}^6}{x^4E^6(1-x)^2},\left(\frac{\boldsymbol{k}}{(1-x)E}\right)^4,\\
&\qquad\frac{\boldsymbol{k}^6}{x^2(1-x)^4E^6},\left(\frac{\boldsymbol{k}}{x(1-x)E^2}\right)^8\Bigg]\Bigg)+\boldsymbol{k}^2\\
&= \frac{\boldsymbol{k}^2}{2x}-\frac{\boldsymbol{k}^2}{2}-\frac{\boldsymbol{k}^4}{4x(1-x)E^2}+\frac{\boldsymbol{k}^2x}{2(1-x)}\\
&\quad-x(1-x)E^2\mathcal{O}\Bigg[\left(\frac{\boldsymbol{k}}{xE}\right)^4,\frac{\boldsymbol{k}^6}{x^4E^6(1-x)^2},\left(\frac{\boldsymbol{k}}{(1-x)E}\right)^4,\\
&\qquad\frac{\boldsymbol{k}^6}{x^2(1-x)^4E^6},\left(\frac{\boldsymbol{k}}{x(1-x)E^2}\right)^8\Bigg]\Bigg)+\boldsymbol{k}^2. \qquad (93)
\end{aligned}
$$

By softness and collinearity, $\boldsymbol{k}^2/2x$ is the dominant term, hence we have that

$$P^2 = 2p\cdot k \simeq \frac{\boldsymbol{k}^2}{x}. \qquad (94)$$

One can similarly show that

$$p\cdot\epsilon^{*\lambda} \simeq \frac{\boldsymbol{k}\cdot\boldsymbol{\epsilon}^{*\lambda}}{x} \qquad (95)$$

Hence,

$$i\mathcal{M} \simeq -2g\frac{\boldsymbol{k}_i\boldsymbol{\epsilon}^{*a\lambda c_\epsilon i}}{\boldsymbol{k}^2}\bar{u}^{s_pc_pj\alpha}(p)t^a_{jl}\left(\mathcal{M}_0\right)_{\alpha\omega\rho\ldots}u^{s_0c_0l\omega}(P_0)(\cdots)^{\rho\cdots}, \tag{96}$$

where $i \in 1, 2$.

Next,

$$(i\mathcal{M})^\dagger \simeq \frac{\boldsymbol{k}_{i'}\boldsymbol{\epsilon}^{b\lambda c_\epsilon i'}}{\boldsymbol{k}^2}(\cdots)^{\rho'\cdots}\bar{u}^{s_0c_0l'\omega'}(P_0)(\mathcal{M}_0^\dagger)_{\alpha'\omega'\rho'\ldots}t^b_{l'j'}u^{s_pc_pj'\alpha'}(p), \tag{97}$$

therefore

$$\begin{aligned}\mathcal{M}\mathcal{M}^\dagger &= |\mathcal{M}|^2 \\ &\simeq 4g^2\frac{\boldsymbol{k}_i\boldsymbol{\epsilon}^{*a\lambda c_\epsilon i}\boldsymbol{k}_{i'}\boldsymbol{\epsilon}^{b\lambda c_\epsilon i'}}{\boldsymbol{k}^4}(\cdots)^{\rho\cdots}(\cdots)^{\rho'\cdots} \\ &\quad\times\left(\mathcal{M}_0\right)_{\alpha\omega\rho\ldots}\left(\mathcal{M}_0^\dagger\right)_{\alpha'\omega'\rho'\ldots}t^a_{jl}t^b_{l'j'} \\ &\quad\times\bar{u}^{s_pc_pj\alpha}(p)u^{s_pc_pj'\alpha'}(p)\bar{u}^{s_0c_0l'\omega'}(P_0)u^{s_0c_0l\omega}(P_0).\end{aligned} \tag{98}$$

Now that we have an expression for $|\mathcal{M}|^2$, we may make progress in computing the average over initial states and sum over final states of the amplitude squared:

$$\left(\frac{1}{2}\sum_{s_0}\right)\left(\frac{1}{N_c}\sum_{c_0}\right)\sum_\lambda\sum_a\sum_b\sum_{s_p}\sum_{c_p}\sum_{c_\epsilon}|\mathcal{M}|^2. \tag{99}$$

From [21], we have that

$$\begin{aligned}\sum_{s_p}\sum_{c_p}\bar{u}^{s_pc_pj\alpha}(p)u^{s_pc_pj'\alpha'}(p) &= \not{p}^{\alpha\alpha'}\delta^{jj'}, \\ \sum_{s_0}\sum_{c_0}\bar{u}^{s_0c_0l'\omega'}(P_0)u^{s_0c_0l\omega}(P_0) &= \not{P}_0^{\omega\omega'}\delta^{ll'}, \text{ and} \\ \sum_a\sum_b\sum_{c_\epsilon}\sum_\lambda\boldsymbol{\epsilon}^{*a\lambda c_\epsilon i}\boldsymbol{\epsilon}^{b\lambda c_\epsilon i'} &= -\eta^{ii'}\delta^{ab} = \delta^{ii'}\delta^{ab}.\end{aligned} \tag{100}$$

Using Eq. (100), we have that

$$\begin{aligned}
&\left(\frac{1}{2}\sum_{s_0}\right)\left(\frac{1}{N_c}\sum_{c_0}\right)\sum_{\lambda}\sum_{a}\sum_{b}\sum_{s_p}\sum_{c_p}\sum_{c_\epsilon}|\mathcal{M}|^2 \\
&\quad\simeq \frac{4g^2}{2N_C}\frac{\boldsymbol{k}_i\boldsymbol{k}_{i'}}{\boldsymbol{k}^4}(\cdots)^{\rho\cdots}(\cdots)^{\rho'\cdots}\left(\mathcal{M}_0\right)_{\alpha\omega\rho\ldots}\left(\mathcal{M}_0^\dagger\right)_{\alpha'\omega'\rho'\ldots} \\
&\qquad\times t^a_{jl}t^b_{l'j'}\not{p}^{\alpha\alpha'}\delta^{jj'}\not{P}_0{}^{\omega\omega'}\delta^{ll'}\delta^{ii'}\delta^{ab} \\
&\quad= \frac{2g^2}{N_C}\frac{1}{\boldsymbol{k}^2}(\cdots)^{\rho\cdots}(\cdots)^{\rho'\cdots}\left(\mathcal{M}_0\right)_{\alpha\omega\rho\ldots}\left(\mathcal{M}_0^\dagger\right)_{\alpha'\omega'\rho'\ldots} \\
&\qquad\times \mathrm{tr}[t^at^a]\not{p}^{\alpha\alpha'}\not{P}_0{}^{\omega\omega'}.
\end{aligned} \tag{101}$$

But $\mathrm{tr}[t^at^b] = T_F\delta^{ab}$, so

$$\mathrm{tr}\left[t^at^a\right] = T_F\delta^{aa} = \frac{N_C^2-1}{2}. \tag{102}$$

Thus,

$$\begin{aligned}
&\left(\frac{1}{2}\sum_{s_0}\right)\left(\frac{1}{N_c}\sum_{c_0}\right)\sum_{\lambda}\sum_{a}\sum_{b}\sum_{s_p}\sum_{c_p}\sum_{c_\epsilon}|\mathcal{M}|^2 \\
&\quad\simeq 2C_Rg^2\frac{1}{\boldsymbol{k}^2}(\cdots)^{\rho\cdots}(\cdots)^{\rho'\cdots}\left(\mathcal{M}_0\right)_{\alpha\omega\rho\ldots}\left(\mathcal{M}_0^\dagger\right)_{\alpha'\omega'\rho'\ldots}\not{p}^{\alpha\alpha'}\not{P}_0{}^{\omega\omega'}.
\end{aligned} \tag{103}$$

In conclusion,

$$\left\langle|\mathcal{M}|^2\right\rangle \simeq 4C_Rg^2\frac{1}{\boldsymbol{k}^2}\left\langle\left|\mathcal{M}_0\left(P,P_0\right)\right|^2\right\rangle. \tag{104}$$

## References


[1] Gyulassy M, Vitev I, Wang X N and Zhang B W 2004 123–191 (*Preprint* nucl-th/0302077)

[2] Adams J *et al.* (STAR) 2005 *Nucl. Phys. A* **757** 102–183 (*Preprint* nucl-ex/0501009)

[3] Arsene I *et al.* (BRAHMS) 2003 *Phys. Rev. Lett.* **91** 072305 (*Preprint* nucl-ex/0307003)

[4] Adler S S *et al.* (PHENIX) 2003 *Phys. Rev. Lett.* **91** 072303 (*Preprint* nucl-ex/0306021)

[5] Back B B *et al.* (PHOBOS) 2003 *Phys. Rev. Lett.* **91** 072302 (*Preprint* nucl-ex/0306025)

[6] Adams J *et al.* (STAR) 2003 *Phys. Rev. Lett.* **91** 072304 (*Preprint* nucl-ex/0306024)

[7] Adams J *et al.* (STAR) 2004 *Phys. Rev. Lett.* **93** 252301 (*Preprint* nucl-ex/0407007)

[8] Adler C *et al.* (STAR) 2003 *Phys. Rev. Lett.* **90** 082302 (*Preprint* nucl-ex/0210033)

[9] Wang F (STAR) 2004 *J. Phys. G* **30** S1299–S1304 (*Preprint* nucl-ex/0404010)

[10] Landau L D and Pomeranchuk I 1953 *Dokl. Akad. Nauk Ser. Fiz.* **92** 535–536

[11] Landau L D and Pomeranchuk I 1953 *Dokl. Akad. Nauk Ser. Fiz.* **92** 735–738

[12] Migdal A B 1956 *Phys. Rev.* **103** 1811–1820

[13] Horowitz W A 2010 *Probing the Frontiers of QCD* Other thesis (*Preprint* 1011.4316)

[14] Armesto N *et al.* 2012 *Phys. Rev. C* **86** 064904 (*Preprint* 1106.1106)

[15] Wiedemann U A 2001 *Nucl. Phys. A* **690** 731–751 (*Preprint* hep-ph/0008241)

[16] Horowitz W A and Cole B A 2010 *Phys. Rev. C* **81** 024909 (*Preprint* 0910.1823)

[17] Caron-Huot S and Gale C 2010 *Phys. Rev. C* **82** 064902 (*Preprint* 1006.2379)

[18] Gyulassy M, Levai P and Vitev I 2002 *Phys. Lett. B* **538** 282–288 (*Preprint* nucl-th/0112071)

[19] Majumder A and Van Leeuwen M 2011 *Prog. Part. Nucl. Phys.* **66** 41–92 (*Preprint* 1002.2206)

[20] Djordjevic M and Gyulassy M 2004 *Nucl. Phys. A* **733** 265–298 (*Preprint* nucl-th/0310076)

[21] Peskin M E and Schroeder D V 1995 *An Introduction to quantum field theory* (Reading, USA: Addison-Wesley) ISBN 978-0-201-50397-5